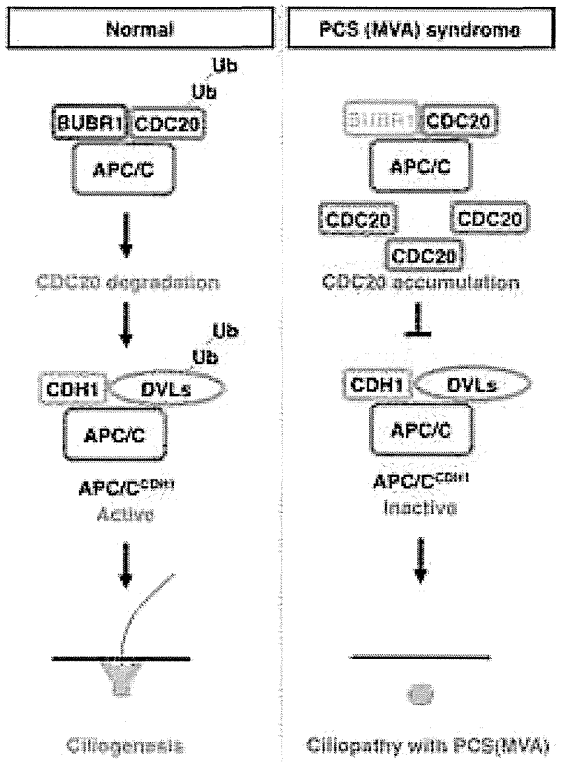

Figure 6. A model of the molecular function of BUBR1 in ciliogenesis. BUBR1-dependent CDC20 degradation in G0 phase cells plays a role in the maintenance of APC/C^{CDH1} activity during primary cilia formation. In PCS (MVA) syndrome cells, insufficiency of BUBR1 results in CDC20 accumulation to inhibit APC/C^{CDH1} activity in G0 phase. Excess amounts of DVLs, the targets of APC/C^{CDH1}, interfere apical docking of centrosomes to cause impaired ciliogenesis.

and specificity are shown in Fig. 7D and Supplementary Material, Figs. 6 and 7) perturbed the formation of the cerebellum (Fig. 7B), as observed in patients with the PCS (MVA) syndrome. *bubr1* morphants also showed perturbed left–right asymmetry of visceral organs including the liver, spleen, gut and cardiac looping (Fig. 7C and D and Supplementary Material, Fig. S7), although no patients with the syndrome with perturbed left–right asymmetry have been reported. Randomized expression of left–right asymmetry genes was observed, including the nodal ligand *southpaw* (*spaw*) and its downstream genes *lefty* and *pitx2* in the lateral plate mesoderm, which comprise the readout of cilium-generated fluid flow in Kupffer's vesicle, a teleost-specific organ equivalent to a mouse node (Supplementary Material, Fig. S8). The number of cilia in Kupffer's vesicle was significantly reduced (Fig. 7E and F), resulting in defective fluid flow (Fig. 7E and G and Supplementary Material, Movies S1 and S2). These results demonstrate a conserved role of BUBR1 for the primary cilium formation, but also suggest phenotypic heterogeneity between human and medaka fish.

DISCUSSION

In mammalian cells, failure of spindle microtubule–kinetochore attachments in M phase activates BUBR1 to bind to CDC20 and inhibit APC/C^{CDC20}, leading to inhibition of chromosome separation (1,2,18,20). Although the inhibition of CDC20 by BUBR1 for spindle assembly checkpoint in M phase has been well established (1–5), the role of BUBR1 in G0 phase was unclear. We found that BUBR1 binds to CDC20 and the core APC/C subunits and forms a complex in G0 phase, and that siRNA-knockdown of BUBR1 in HEK293T cells impairs poly-ubiquitination of CDC20. These results demonstrate that in G0 phase BUBR1 inhibits APC/C^{CDC20} activity through the proteasomal degradation of CDC20. Accumulation of CDC20 was observed in the PCS (MVA) syndrome cells, but was not likely to be the mitotic leakage, because in late M phase active APC/C^{CDC20} causes its own inhibition and switches to APC/C^{CDH1} activity independently of spindle assembly checkpoint (21). It was recently reported that BUBR1 binds to CDC20 to inhibit APC/C^{CDC20} in interphase, thereby allowing accumulation of cyclin B in G2 phase prior to mitotic onset (4,5). Thus, BUBR1 may function as an inhibitor of APC/C^{CDC20} not only in early M phase but also in multiple phases of the cell cycle.

Conditional knockdown of *APC2*, a core subunit of APC/C, in G0-quiescent hepatocytes in mice caused dedifferentiation and unscheduled proliferation of these cells, which may be attributed to the lack of APC/C^{CDH1} activity (22). APC/C^{CDH1} activity regulates axonal growth in postmitotic neurons (23). In the context of cilia formation, APC/C^{CDH1} activity is indispensable for apical docking of basal body through the quantitative regulation of DVL by APC/C^{CDH1} in *Xenopus* embryos (9). CDC14 phosphatases in vertebrates, *CDC14A* and *CDC14B*, both counteract CDH1 phosphorylation to activate APC/C^{CDH1} activity during late M phase (24). Loss of *CDC14B* in zebrafish embryos caused ciliary dysfunction characterized by hydrocephaly, kidney cysts and left–right asymmetry defects (25). These findings suggested that APC/C^{CDH1} activity in G0 phase is essential for cell differentiation and cell morphology (26). In spite of the functional significance of APC/C^{CDH1}, the maintenance mechanism in G0 phase was unclear. We showed that the accumulation of CDC20 in G0 phase interferes with the APC/C^{CDH1}-mediated proteolysis of DVL for ciliogenesis, and that BUBR1 is required for the maintenance of the APC/C^{CDH1} activity in G0 phase.

The 'APC/C^{CDH1}–DVL proteolysis' axis in G0 phase is fundamental for ciliogenesis. Our data demonstrated that BUBR1 in G0 phase maintains the APC/C^{CDH1} activity to establish the 'BUBR1–APC/C^{CDH1}–DVL proteolysis' axis for ciliogenesis. It was reported that inversin (NPHP2), an underlying protein for the ciliopathy in both human and mouse, binds to DVL and promotes the ubiquitination of DVL by APC/C^{CDH1} (15). Loss of *inversin* leads to increased amounts of DVL and ciliary dysfunction similarly to the PCS (MVA) syndrome. Therefore, the PCS (MVA) syndrome and inversin-mutated ciliopathy (nephronophthisis) may have a common pathological pathway, and BUBR1 may act epistatically upstream of both inversin and DVL to maintain APC/C^{CDH1} activity for ciliogenesis, because inversin is also a direct substrate of APC/C^{CDH1} (15).

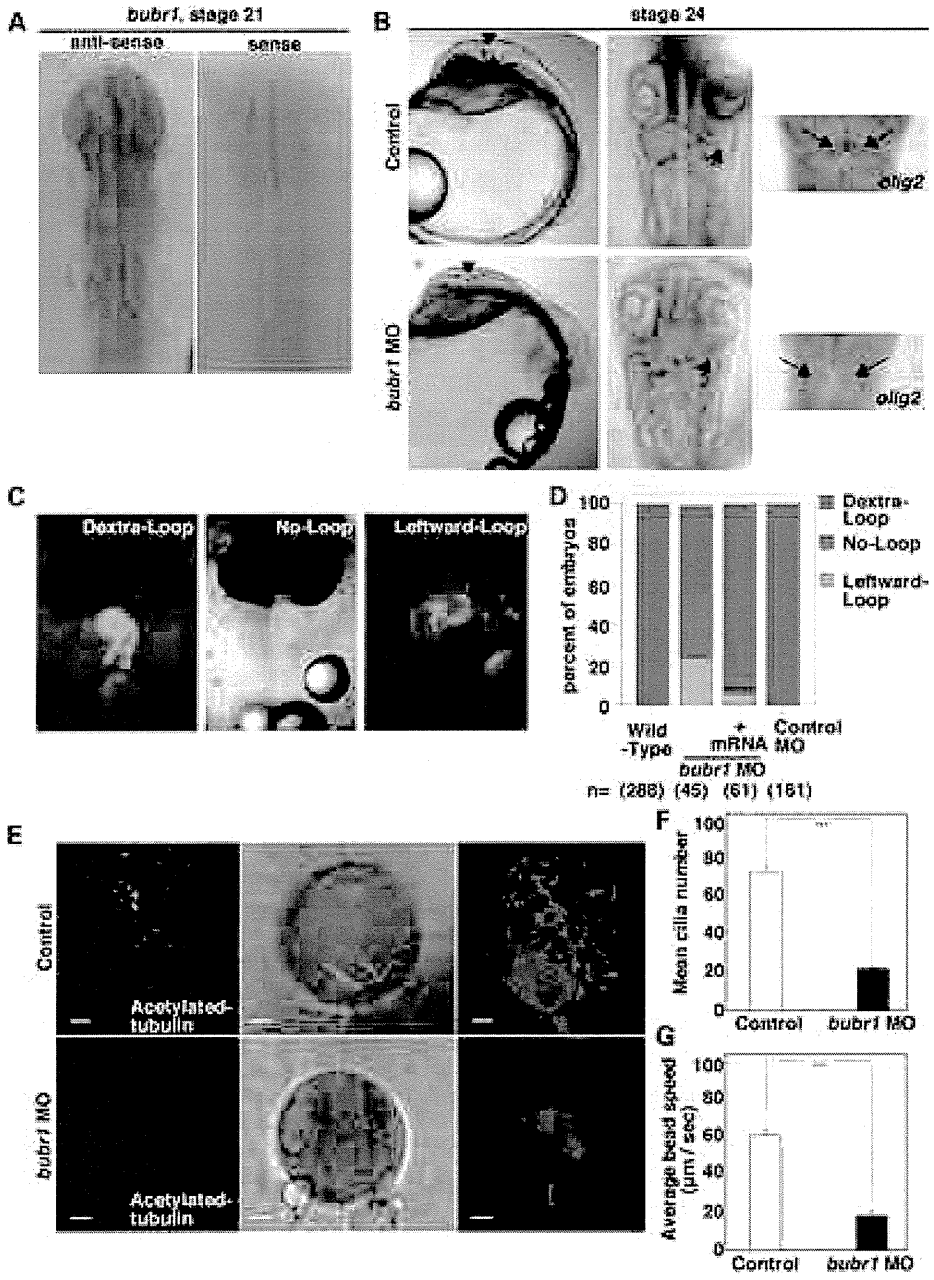

Figure 7. Morpholino knockdown of *bubr1* in medaka fish causes ciliary dysfunction. (**A**) Left panel shows ubiquitous expression of *bubr1* at stage 21 (six somites). Right panel is a negative control for *in situ* hybridization of *bubr1*. (**B**) Phenotypes of medaka *bubr1* morphants (MO). Lateral views of whole body and dorsal views of head formation at stage 24 (16 somites). *bubr1* morphants (6 of 26 injected embryos) exhibit reduction of the mid-hindbrain (arrowheads). Cerebellum (arrows) detected by *olig2* expression. *bubr1* morphants (22/28) show defective cerebellar development. (**C**) Heart laterality defects in *bubr1* morphants. Randomized heart looping in *bubr1* morphants was partially rescued in *bubr1* mRNA co-injected embryos. Images of normal heart looping (Dextra-Loop), no heart looping and reversed heart looping (Leftward-Loop) in frontal views of *cmcl2*-enhanced green fluorescent protein (EGFP)-labelled hearts at stage 28 (30 somites). (**D**) A graph showing the proportion of *bubr1* morphants displaying laterality defects in the heart. (**E**–**G**) Ciliary defects in Kupffer's vesicle (KV) of a *bubr1* morphant. Confocal images of embryos at stage 21 showing the KV labelled with an anti-acetylated-tubulin antibody (bars: 80 μm), and the statistics of the number.*bubr1* morphants ($n = 5$) have fewer cilia than controls ($n = 7$) (F). The statistical significance of the differences was examined by *t*-tests. $^{***}P < 0.01$. Bright-field and Z-stack projections (red) of fluorescent time-lapse images of KVs injected with fluorescent beads at stage 21(bars: 10 μm) are shown in the middle and right panels, respectively (E). Coloured lines in middle panel indicate representative bead trajectories. In wild-type KVs, a general counter-clockwise flow is observed ($n = 7$; see Supplementary Material, Movie S1). In morphants, only random Brownian motion is observed ($n = 7$; see Supplementary Material, Movie S2) (bars: 10 μm). The bead speeds are much slower in *bubr1* morphants than in control morpholino-injected embryos (G).

Ciliogenesis is regulated dynamically in a cell cycle-dependent manner (27). While ciliogenesis occurs in G0/G1 phase, cilia disassembly begins when G0-quiescent cells re-enter the cell cycle and become irreversibly committed to DNA replication in late G1 phase (27,28). We showed that BUBR1, a cell cycle regulator, plays a crucial role in cilia formation through the quantitative regulation of ciliary protein. It was also reported that some ciliary molecules control cell division program. In *Chlamydomonas*, IFT27, a Rab-like small G protein, is required for both cell proliferation and flagellum formation (29). A complex of two centrosomal proteins, CP110 and CEP92, promotes cell cycle progression and cilia disassembly in mammalian cells (30). Polycystin-1, -2 and polaris mediate chromosome segregation through the proper expression of survivin, a chromosome passenger protein (31). Thus, cross talk between cell cycle regulators and ciliogenesis machineries is essential for the cell cycle-dependent ciliary dynamics.

Both monoallelic and biallelic mutations of *BUB1B* have been found in individuals with the PCS (MVA) syndrome (7,8). Patients with monoallelic mutations were severely affected with the Dandy–Walker complex (9/11 patients), polycystic nephroblastoma (7/11) and rhabdomyosarcoma (5/11). On the other hand, patients with biallelic mutations showed a moderate phenotype: Dandy–Walker complex (0/5 patients), polycystic nephroblastoma (0/5) and rhabdomyosarcoma (2/5). These results suggest a possible correlation of *BUB1B* mutations with ciliopathy and cancer phenotypes.

In summary, our data demonstrate that BUBR1 is required for the maintenance of APC/C^{CDH1} activity in G0 phase, and that failure of the maintenance of APC/C^{CDH1} activity is responsible for the impaired ciliogenesis of the PCS (MVA) syndrome.

MATERIALS AND METHODS

Cell culture

The immortalized fibroblast cell lines from two patients with the PCS (MVA) syndrome (PCS1 and MY1), a fibroblast cell line from a normal individual (SM) and a chromosome 15-transferred PCS1 cells (PCS1-Ch.15) were described previously (8,13,14). In brief, the MY1 cell line was derived from patient 2 with a heterozygous intronic mutation IVS10-5A > G in *BUB1B*, which results in an aberrant splicing leading to a premature stop codon (W468fsX480) (8). The PCS1 cell line was established from patient 1 with a heterozygous single-base deletion 1833delT, which results in protein truncation (F611fsX625) (8). Although no mutation was found in the second alleles of the two patients, a conserved haplotype around *BUB1B* that links to a modest decrease of their transcripts was observed (8). All cell cultures were maintained in Dulbecco's modified eagle medium (DMEM) supplemented with 10% fetal bovine serum (FBS) at 37°C under 5% CO_2. Transfection of plasmids or siRNAs into cells was performed using the Lipofectamine 2000 reagent (Invitrogen) according to the manufacturer's protocol. At 24 h after transfection, the medium was replaced with serum-free DMEM, and the cells were incubated for 24 h to become Ki-67-negative and achieve quiescent G0 phase.

Antibodies

The primary antibodies used were: mouse anti-acetylated tubulin monoclonal antibody (mAb) (Sigma); rabbit anti-Pericentrin polyclonal antibody (pAb) (Bethyl Laboratories); rat anti-β-tubulin mAb (Novus); mouse anti-β-tubulin mAb (Sigma); mouse anti-active β-catenin (clone 8E7) mAb (Millipore); mouse anti-β-catenin mAb (BD Transduction Laboratories); mouse anti-GAPDH mAb (Santa Cruz Biotechnology); mouse anti-RPA mAb (BD Transduction Laboratories); mouse anti-DVL1 mAb (Santa Cruz Biotechnology); rabbit anti-DVL2 mAb (Cell Signaling Technology Inc.); rabbit anti-DVL3 mAb (Cell Signaling Technology Inc.); rabbit anti-CDC20 pAb (Santa Cruz Biotechnology); mouse anti-CDH1 mAb (Thermo); mouse anti-APC2 mAb (Thermo); mouse anti-CDC27 mAb (BD Transduction Laboratories); mouse anti-Cyclin B1 mAb (BD Transduction Laboratories); mouse anti-polyubiquitinated proteins (clone FK1) mAb (Biomol); rabbit anti-GFP pAb (MBL); mouse anti-GFP mAb (Roche); mouse anti-DYKDDDDK (FLAG) tag mAb (Wako) and rabbit anti-hemagglutinin (HA) pAb (Santa Cruz Biotechnology). The rabbit anti-human BUBR1 pAb was raised and characterized previously (8,14).

Plasmids

HA-tagged mouse DVL2 and enhanced green fluorescent protein (EGFP)-tagged human BUBR1 were described previously (14,32). We constructed a FLAG-tagged mouse DVL2 plasmid by polymerase chain reaction (PCR) and standard cloning techniques. We used site-directed mutagenesis to insert mutations into DVL2 and BUBR1. The mutations were verified by automated sequencing.

Electron microscopy

Cells cultured on polycarbonate filters (Corning) were fixed with 4% paraformaldehyde and 2% glutaraldehyde in 0.1 M cacodylated buffer (pH 7.4) for 10 min at 37°C and then washed with 0.1 M phosphate buffer. Samples were post-fixed in 2% OsO_4 in the same buffer for 90 min on ice, dehydrated in ethanol and embedded in Epon 812. Thin sections were cut, double-stained with uranyl acetate and lead citrate for 4 min at room temperature and examined under an electron microscope (JEM-1200EX; Jeol) at an accelerating voltage of 80 kV.

RNA interference

The following stealth siRNAs synthesized by Invitrogen were used: human *BUB1B*-1 (5′-UCAAGGGUUCAAUUCCUUCCUGUAAAUUC-3′); human *BUB1B*-2 (5′-AUACCAAACAGGUCUACCUGGUAGG-3′); dog *BUB1B*-1 (5′-UGGAGAUACAUCCUCAUUGGAGUUG-3′); dog *BUB1B*-2 (5′-AUCACUGGCAUUCAGAAUCCGCACA-3′); human *CDC20*-1 (5′-UUUGAGUUCAGCCACCUUGGCCAUG-3′) and human *CDC20*-2 (5′-AUUACCACCACUGGCCAAAUGUCGU-3′). Human *DVL2/DVL3* siRNA (5′-GUCAACAAGAUCACCUUCUTT-3′) synthesized by QIAGEN was used.

Stealth-negative control duplexes (Cat. No. 12935-300 and 12935-112; Invitrogen) were also used.

Immunoprecipitation and western blot analyses

Cells were transfected with siRNAs or plasmid DNA, and cultured in serum-free DMEM for 24 h. The cells were lysed in lysis buffer (0.5% Triton X-100, 150 mM NaCl, 20 mM Tris–HCl pH 7.5, 1 mM ethylene-diamine-tetraacetic acid (EDTA), 0.5 mM phenyl-methyl-sulfonyl fluoride (PMSF), 2 mg/ml pepstatin A, 10 mg/ml leupeptin, 5 mg/ml aprotinin). The lysates were sheared with a 21-gauge needle, incubated on ice for 30 min and clarified by centrifugation at 20,817*g* for 15 min at 4°C. The supernatants were pre-cleared with protein A/G-conjugated agarose and incubated with anti-FLAG, anti-DVL2 or anti-GFP antibodies for 2 h at 4°C with constant rotation. Protein A/G-conjugated agarose was then added to the lysates and the mixtures were rotated for a further 12 h at 4°C. The agarose beads were washed three times with wash buffer (1% Nonidet P-40, 0.1% SDS, 0.5% deoxycholate, 150 mM NaCl, 50 mM Tris–HCl pH 7.5, 1 mM EDTA, 0.5 mM PMSF, 2 mg/ml pepstatin A, 10 mg/ml leupeptin, 5 mg/ml aprotinin) before elution with sample buffer. The immunoprecipitated proteins were analysed by 10% sodium dodecyl sulfate-polyacrylamide gel electrophoresis (SDS-PAGE) and transferred to polyvinylidene fluoride membranes for immunoblotting analyses.

Immunofluorescence microscopy

Cells grown on cover slips were fixed in 100% methanol at −20°C for 10 min, briefly washed with phosphate buffered saline (PBS) three times, blocked with 1% bovine serum albumin (BSA) in PBS for 30 min and probed with primary antibodies. Antibody–antigen complexes were detected with Alexa Fluor 594- or Alexa Fluor 488-conjugated goat secondary antibodies (Molecular Probes) by incubation for 30 min at room temperature. The cells were washed three times with PBS and then counterstained with 4′,6′-diamidino-2-phenylindole (DAPI). Immunostained cells were examined under a fluorescence microscope (Zeiss Axioskop2; Carl Zeiss Microimaging Inc.) and a confocal microscope (FV1000-D; Olympus Inc.).

Protein half-life assay

Cells were treated with 25 mg/ml Chx for 0, 2 or 4 h to determine the half-life of DVL2. To inhibit proteasome-dependent degradation, cells were treated with 5 mM MG132 (Sigma) for 5 h before harvesting.

Cell fractionation

Cytoplasmic and nuclear extracts were prepared using a Cel-Lytic NuCLEAR Extraction Kit (Sigma) according to the manufacturer's protocol.

Cell-cycle synchronization

Cells were synchronized at the G1/S phase boundary by double-thymidine block, and at the G0 phase by serum starvation. For thymidine block, cells were incubated with 2 mM thymidine for 16 h, washed extensively with DMEM supplemented with 10% FBS, released for 8 h and subjected to a second thymidine block for 18 h and released.

Luciferase assay

Cells (1×10^5) were plated in 12-well plates. On the following day, the cells were transfected with 200 ng of Topflash or Fopflash luciferase reporter plasmid (Upstate Biotechnology) plus 2 ng of internal control plasmid pRL-TK (Promega) using the Lipofectamine 2000 reagent (Invitrogen). The transfected cells were lysed and analysed for their relative β-catenin/Tcf activities using a Dual-Luciferase Reporter Assay System (Promega). To inhibit Wnt/β-catenin signalling, 10 μM FH535 (Sigma) or 40 μM IWR-1 (Sigma) were added to the media at 24 h before luciferase assay.

Medaka fish maintenance

Embryos of the Kyoto-Cab inbred medaka strain were used for all experiments (19). To visualize left–right asymmetry of the heart, the *cmcl2*-EGFP transgenic medaka line was used. Microinjection, raising and staging were carried out as previously described (33).

Morpholino oligonucleotides and mRNA injections

The following morpholinos against two distinct domains of medaka *bubr1* pre-mRNA synthesized by Gene Tools LLC were used: translation-blocking morpholino (TBMO), 5′-ATTCCACATCACCACCTTCCGCCAT-3′; and splice-blocking morpholino (SBMO), 5′-TATATCTGTAAGGAGTCAACCAGGT-3′. For negative controls, a standard control morpholino (5′-CCTCTTACCTCAGTTACAATTTATA-3′) was used. A volume of 1 nl was injected with 5 ng of SBMO, 1.5 ng of TBMO or an equivalent amount of control morpholinos to each *bubr1* morphant.

Capped medaka *bubr1* mRNA was synthesized using an mMessage Machine SP6 Transcription Kit (Ambion) from the full-length medaka *bubr1* cDNA in pCS2+ cloned by RT–PCR. For rescue experiments, 100 pg of *bubr1* mRNA was coinjected with 1.5 ng of *bubr1* TBMO into one-cell-stage embryos.

RT–PCR

Total RNA was extracted from 10 each of wild-type or SBMO (5 ng)-injected embryo pools using the TRIzol reagent (Invitrogen) according to the manufacturer's protocol. First-strand cDNAs were generated with an oligo (dT) primer using an RNA PCR™ Kit (AMV) Ver. 3.0 (Takara Bio Inc.). To examine the efficacy of the SBMO targeted toward the intron–exon boundary of exon 4, primers spanning exon 3 (5′-AGACGATCCTCTTGGTGTT-3′) and exon 5 (5′-TTTGCGAAAGTTGCCCTG-3′) were designed. PCR amplification was performed with TaKaRa Ex Taq HS (Takara Bio Inc.) using the cDNAs from the wild-type and morpholino-injected embryos in three independent experiments.

In situ hybridization

Whole-mount *in situ* hybridization analyses were carried out as described previously (33). Digoxigenin-labelled RNA probes were generated using a DIG RNA Labeling Kit (Roche). cDNA templates for *bubr1*, *spaw*, *lefty*, *pitx2* and *olig2* were cloned into pBluescript SK- by RT–PCR.

Analysis of Kupffer's vesicle (KV) flow

Dechorionated embryos were mounted in 1.5% low-melting agarose. Fluorescent beads (1.0 μm; Invitrogen) were injected into KVs and imaged using an MZ16FA microscope (Leica) with a DFC350FX digital camera. The bead trajectories were traced by sequential time-lapse images using ImageJ 1.42q software (NIH).

Imaging of cilia in KVs

Ciliogenesis in medaka embyos was analysed by both immunohistochemistry and live imaging. Whole-mount antibody staining was performed as previously described (33). The antibodies used were an anti-acetylated α-tubulin antibody (1:200; Sigma T-6793) and an Alexa Fluor 488-conjugated anti-mouse IgG secondary antibody (1:500; Invitrogen). For live imaging of cilia, mARL13b-GFP mRNA (34) was injected into 1-cell-stage embryos and dechorionated embryos at stage 21 (34 hpf) were used. Immunostained or mRNA-injected embryos were mounted in agarose and imaged using an SP2 confocal microscope (Leica).

The number of cilia was quantified by counting every cilium in the tissue of interest using ImageJ 1.42q software (NIH). SPSS software ver. 16.0 (SPSS Inc.) was used to carry out two-sample *t*-tests to compare the cilia numbers in tissues of interest in TBMO-injected embryos with those in uninjected wild-type embryos. Values of $P < 0.01$ were considered to be statistically significant.

Statistical analysis

The experiments were performed at least three times, and the data are shown as means ± standard error of the mean. Statistical analyses were performed using StatView software (SAS Institute). Differences between the data were tested for statistical significance using Student's *t*-test. Values of $P < 0.05$ were considered to be statistically significant.

SUPPLEMENTARY MATERIAL

Supplementary Material is available at *HMG* online.

ACKNOWLEDGEMENTS

We thank M. Kobayashi, T. Takumi and S. Horita for providing clinical information, and C. Tickle, F. Bangs, S. Bagby and L. Hurst (University of Bath) for valuable comments and critical reading of the manuscript. We also thank Y. Tonouchi for technical support and K. Koike (Center for Gene Science, Hiroshima University) for electron microscopy observations.

Conflict of Interest statement. None declared.

FUNDING

This work was supported by a Grant-in-Aid for Scientific Research (to S.M.) and a Grant-in-Aid for Cancer Research (to S.M. and T.M.) from the Ministry of Education, Culture, Sports, Science and Technology of Japan, a Hiroshima University Support Foundation grant (to T.M.) and a Hiroshima University Fujii Memorial Foundation grant (to T.M.). M.F.-S. was supported by a senior fellowship from the Medical Research Council (MRC) and S.P. was supported by a DT fellowship from Biotechnology and Biological Sciences Research Council (BBSRC).

REFERENCES

1. Baker, D.J., Chen, J. and van Deursen, J.M.A. (2005) The mitotic checkpoint in cancer and aging: what have mice taught us? *Curr. Opin. Cell Biol.*, **17**, 583–589.
2. Sullivan, M. and Morgan, D.O. (2007) Finishing mitosis, one step at a time. *Nat. Rev. Mol. Cell Biol.*, **8**, 894–903.
3. Choi, E., Choe, H., Min, J., Choi, J.Y., Kim, J. and Lee, H. (2009) BubR1 acetylation at prometaphase is required for modulating APC/C activity and timing of mitosis. *EMBO J.*, **28**, 2077–2089.
4. Kulukian, A., Han, J.S. and Cleveland, D.W. (2009) Unattached kinetochores catalyze production of an anaphase inhibitor that requires a Mad2 template to prime Cdc20 for BubR1 binding. *Dev. Cell*, **16**, 105–117.
5. Malureanu, L.A., Jeganathan, K.B., Hamada, M., Wasilewski, L., Davenport, J. and van Deursen, J.M. (2009) BubR1 N terminus acts as a soluble inhibitor of cyclin B degradation by APC/C(Cdc20) in interphase. *Dev. Cell*, **16**, 118–131.
6. Peters, J.M. (2006) The anaphase promoting complex/cyclosome: a machine designed to destroy. *Nat. Rev. Mol. Cell Biol.*, **7**, 644–656.
7. Hanks, S., Coleman, K., Reid, S., Plaja, A., Firth, H., Fitzpatrick, D., Kidd, A., Méhes, K., Nash, R., Robin, N. *et al.* (2004) Constitutional aneuploidy and cancer predisposition caused by biallelic mutations in BUB1B. *Nat. Genet.*, **36**, 1159–1161.
8. Matsuura, S., Matsumoto, Y., Morishima, K.-I., Izumi, H., Matsumoto, H., Ito, E., Tsutsui, K., Kobayashi, J., Tauchi, H., Kajiwara, Y. *et al.* (2006) Monoallelic BUB1B mutations and defective mitotic-spindle checkpoint in seven families with premature chromatid separation (PCS) syndrome. *Am. J. Med. Genet. A*, **140**, 358–367.
9. Ganner, A., Lienkamp, S., Schäfer, T., Romaker, D., Wegierski, T., Park, T.J., Spreitzer, S., Simons, M., Gloy, J., Kim, E. *et al.* (2009) Regulation of ciliary polarity by the APC/C. *Proc. Natl Acad. Sci. USA*, **106**, 17799–17804.
10. Gerdes, J.M., Davis, E.E. and Katsanis, N. (2009) The vertebrate primary cilium in development, homeostasis, and disease. *Cell*, **137**, 32–45.
11. Goetz, S.C. and Anderson, K.V. (2010) The primary cilium: a signalling centre during vertebrate development. *Nat. Rev. Genet.*, **11**, 331–344.
12. Nigg, E.A. and Raff, J.W. (2009) Centrioles, centrosomes, and cilia in health and disease. *Cell*, **139**, 663–678.
13. Matsuura, S., Ito, E., Tauchi, H., Komatsu, K., Ikeuchi, T. and Kajii, T. (2000) Chromosomal instability syndrome of total premature chromatid separation with mosaic variegated aneuploidy is defective in mitotic-spindle checkpoint. *Am. J. Hum. Genet.*, **67**, 483–486.
14. Izumi, H., Matsumoto, Y., Ikeuchi, T., Saya, H., Kajii, T. and Matsuura, S. (2009) BubR1 localizes to centrosomes and suppresses centrosome amplification via regulating Plk1 activity in interphase cells. *Oncogene*, **28**, 2806–2820.
15. Simons, M., Gloy, J., Ganner, A., Bullerkotte, A., Bashkurov, M., Krönig, C., Schermer, B., Benzing, T., Cabello, O.A., Jenny, A. *et al.* (2005) Inversin, the gene product mutated in nephronophthisis type II, functions as a molecular switch between Wnt signaling pathways. *Nat. Genet.*, **37**, 537–543.
16. Park, T.J., Mitchell, B.J., Abitua, P.B., Kintner, C. and Wallingford, J.B. (2008) Dishevelled controls apical docking and planar polarization of basal bodies in ciliated epithelial cells. *Nat. Genet.*, **40**, 871–879.

17. Listovsky, T., Oren, Y.S., Yudkovsky, Y., Mahbubani, H.M., Weiss, A.M., Lebendiker, M. and Brandeis, M. (2004) Mammalian Cdh1/Fzr mediates its own degradation. *EMBO J.*, **23**, 1619–1626.
18. Nilsson, J., Yekezare, M., Minshull, J. and Pines, J. (2008) The APC/C maintains the spindle assembly checkpoint by targeting Cdc20 for destruction. *Nat. Cell Biol.*, **10**, 1411–1420.
19. Furutani-Seiki, M. and Wittbrodt, J. (2004) Medaka and zebrafish, an evolutionary twin study. *Mech. Dev.*, **121**, 629–637.
20. Yu, H. (2007) Cdc20: a WD40 activator for a cell cycle degradation machine. *Mol. Cell*, **27**, 3–16.
21. Shirayama, M., Toth, A., Galova, M. and Nasmyth, K. (1999) APC(Cdc20) promotes exit from mitosis by destroying the anaphase inhibitor Pds1 and cyclin Clb5. *Nature*, **402**, 203–207.
22. Wirth, K.G., Ricci, R., Gimenez-Abian, J.F., Taghybeeglu, S., Kudo, N.R., Jochum, W., Vasseur-Cognet, M. and Nasmyth, K. (2004) Loss of the anaphase-promoting complex in quiescent cells causes unscheduled hepatocyte proliferation. *Genes Dev.*, **18**, 88–98.
23. Konishi, Y., Stegmuller, J., Matsuda, T., Bonni, S. and Bonni, A. (2004) Cdh1-APC controls axonal growth and patterning in the mammalian brain. *Science*, **303**, 1026–1030.
24. Jaspersen, S.L., Charles, J.F. and Morgan, D.O. (1999) Inhibitory phosphorylation of the APC regulator Hct1 is controlled by the kinase Cdc28 and the phosphatase Cdc14. *Curr. Biol.*, **9**, 227–236.
25. Clement, A., Solnica-Krezel, L. and Gould, K.L. (2011) The Cdc14B phosphatase contributes to ciliogenesis in zebrafish. *Development*, **138**, 291–302.
26. Wasch, R., Robbins, J.A. and Cross, F.R. (2010) The emerging role of APC/CCdh1 in controlling differentiation, genomic stability and tumor suppression. *Oncogene*, **29**, 1–10.
27. Tucker, R.W., Pardee, A.B. and Fujiwara, K. (1979) Centriole ciliation is related to quiescence and DNA synthesis in 3T3 cells. *Cell*, **17**, 527–535.
28. Rieder, C.L., Jensen, C.G. and Jensen, L.C. (1979) The resorption of primary cilia during mitosis in a vertebrate (PtK1) cell line. *J. Ultrastruct. Res.*, **68**, 173–185.
29. Qin, H., Wang, Z., Diener, D. and Rosenbaum, J. (2007) Intraflagellar transport protein 27 is a small G protein involved in cell-cycle control. *Curr. Biol.*, **17**, 193–202.
30. Spektor, A., Tsang, W.Y., Khoo, D. and Dynlacht, B.D. (2007) Cep97 and CP110 suppress a cilia assembly program. *Cell*, **130**, 678–690.
31. Aboualaiwi, W.A., Ratnam, S., Booth, R.L., Shah, J.V. and Nauli, S.M. (2011) Endothelial cells from humans and mice with polycystic kidney disease are characterized by polyploidy and chromosome segregation defects through survivin down-regulation. *Hum. Mol. Genet.*, **20**, 354–367.
32. Kishida, S., Hamao, K., Inoue, M., Hasegawa, M., Matsuura, Y., Mikoshiba, K., Fukuda, M. and Kikuchi, A. (2007) Dvl regulates endo- and exocytotic processes through binding to synaptotagmin. *Genes Cells*, **12**, 49–61.
33. Porazinski, SR, Wang, H. and Furutani-Seiki, M. (2011) Essential techniques for introducing medaka to a zebrafish laboratory—toward combined use of medaka and zebrafish for further genetic dissection of the function of the vertebrate genome. *'Vertebrate embryogenesis, Methods and Protocols' in the series Methods in Molecular Biology*. Humana Press (in press).
34. Borovina, A., Superina, S., Voskas, D. and Ciruna, B. (2010) Vangl2 directs the posterior tilting and asymmetric localization of motile primary cilia. *Nat. Cell Biol.*, **12**, 407–412.

Simpson–Golabi–Behmel syndrome diagnosed by postmortem magnetic resonance imaging, restricted autopsy, and molecular genetics: a case report

Dear Editor,

Simpson–Golabi–Behmel syndrome (SGBS) is an X-linked disorder characterized by an overgrowth syndrome that includes coarse face, congenital heart defects, congenital diaphragmatic hernia (CDH), genitourinary defects, gastrointestinal anomalies, and vertebral/rib anomalies [1,2]. SGBS is diagnosed based on clinical findings, family history, and genetic testing for glypicans (GPC) 3 and 4 [1,2]. Clinical findings should be used to diagnose SGBS when genetic testing is not possible. We describe a case of SGBS terminated at 20 weeks' gestation that was clinically diagnosed by postmortem magnetic resonance imaging (MRI) and autopsy and subsequently confirmed by genetic analysis.

A 30-year-old woman (para 2 + 0) was referred at 8 weeks' gestation because her elder son had SGBS, although her younger son was unaffected. The affected son weighed 2850 g at birth at 32 weeks' gestation. He was diagnosed with SGBS based on clinical manifestations of overgrowth syndrome, trigonocephaly, coarse face, cleft palate, postaxial polydactyly, rib anomalies (13 ribs), and cryptorchidism, but no GPC3 gene mutation was detected.

In the current pregnancy, first-trimester ultrasonography indicated a singleton fetus whose gestational age was consistent with dates based on the last menstrual period. At 18 weeks' gestation, ultrasonography indicated CDH, renal pelvis dilation to 15 mm, male sex, and overgrowth syndrome (estimated fetal body weight, biparietal diameter, head circumference, and abdominal circumference of 99th, 96th, 97th and 95th percentile, respectively), which suggested SGBS. The pregnancy was terminated at 20 weeks' gestation and a 445 g stillborn male was delivered.

The infant had low-set ears, but did not display a large cleft palate, postaxial polydactyly or supernumerary nipples—characteristic findings of SGBS. Since the parents requested that the autopsy be restricted to the chest and abdomen, postmortem MRI was performed before the autopsy, which indicated normal brain structure, small cleft palate (Fig. 1A), large tongue, rib anomalies (13 ribs), renal pelvis dilation, and CDH associated with hepatomegaly (Fig. 1B). The only additional finding detected by autopsy was mesenterium commune (Table 1). He was clinically diagnosed with SGBS by a specialist in dysmorphology (H.O.). Multiplex ligation-dependent probe amplification analysis of the stillborn child and the affected son detected duplication in the GPC3 exon 2b domain (Fig. 2A and B). Duplication in the same domain of the affected son was also confirmed by array-comparative genomic hybridization (Fig. 2C).

Of the overgrowth syndromes, including SGBS, Beckwith–Wiedemann syndrome, Perlman syndrome, Sotos syndrome, and Weaver syndrome [1,2], the clinical features of this case were most consistent with SGBS [1,2]. In this case, the findings of cleft palate and rib anomalies detected by postmortem MRI were essential in differentiating between SGBS and other overgrowth syndromes, particularly Beckwith–Wiedemann syndrome, which has many clinical similarities.

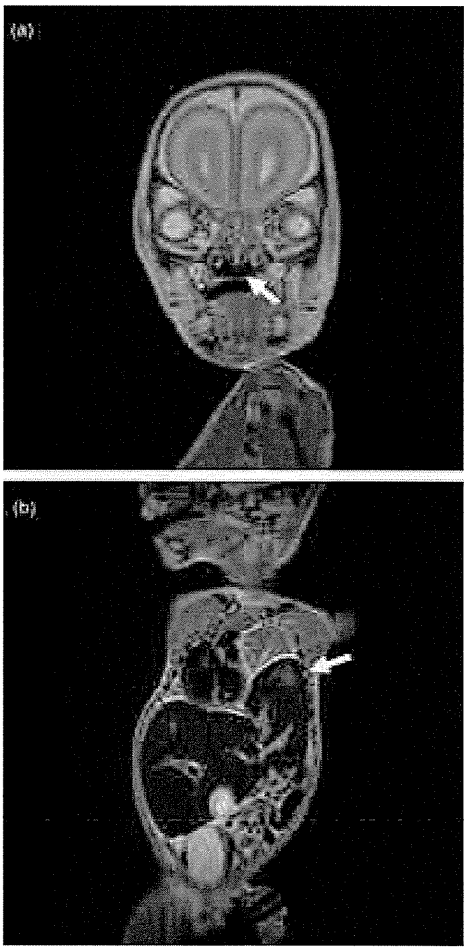

Fig. 1. T2-weighted postmortem magnetic resonance imaging (MRI). Coronal view of the face demonstrates a small palatal fissure (A). Coronal view of the chest and abdomen shows a congenital diaphragmatic hernia (B). We used a two-dimensional T2-weighted fast-spin echo sequence with a 1.5 T scanner. MRI parameters were as follows: TR, 4800 ms; TE, 120 ms; field of view, 15 cm × 15 cm; matrix, 192 × 256; slice, 2 mm; and scan time, 3 min.

Postmortem MRI is a noninvasive tool for detecting a small abnormality, such as a small cleft palate, that may be overlooked on an invasive autopsy. Whole-body postmortem three-dimensional MRI, along with a minimally invasive postmortem examination, has been shown to provide similar information to that of

Table 1
Pathological abnormalities identified by external examination, postmortem magnetic resonance imaging, and restricted autopsy.

	External examination	Postmortem MRI	Restricted autopsy
Overgrowth	*		
Low set ears	*	*	
Cleft palate		*	
Large tongue	*	*	
Congenital diaphragmatic hernia		*	*
Hepatomegary		*	*
Dilation of renal pelvis		*	*
Rib anomalies		*	*
Mesenterium commune			*

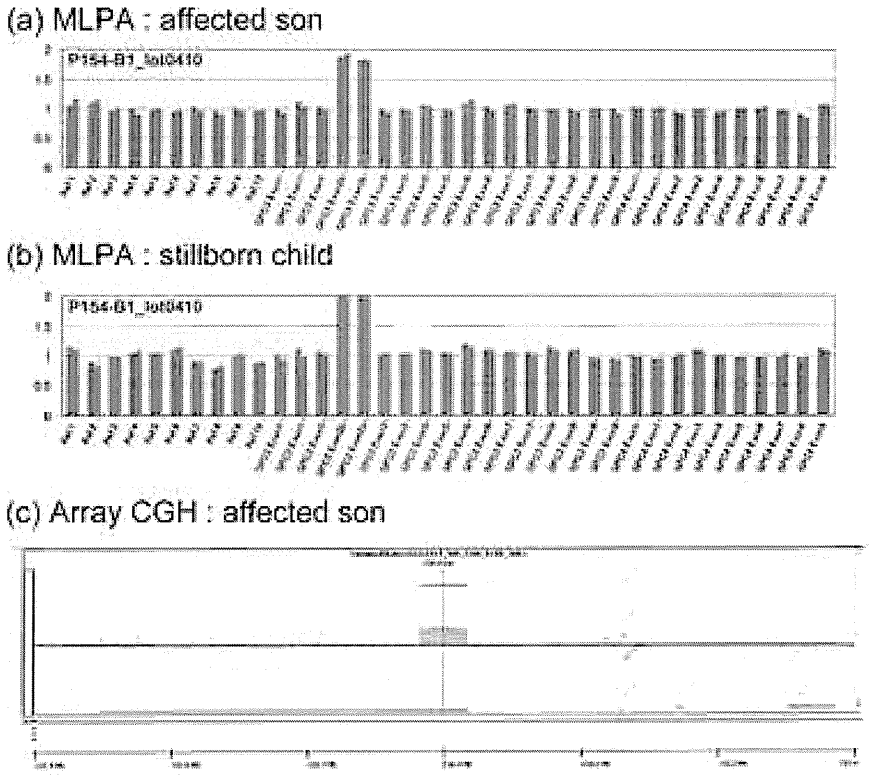

Fig. 2. Genetic analysis of the stillborn child and the affected son. Multiplex ligation-dependent probe amplification analysis detected duplication in the GPC3 exon 2b domain (A and B). Duplication in the same domain was also confirmed in the affected son by array-comparative genomic hybridization (C).

conventional autopsy in fetuses and newborns [3,4]. Moreover, not all patients have access to hospitals with experts in the relevant subspecialties, such as dysmorphology, pediatric radiology, perinatology, and genetics. Postmortem MRI is potentially useful for correct diagnosis of rare multiple congenital anomaly syndromes.

In this case, duplication in the GPC3 domain was confirmed. Although mutations in the GPC3 gene have been believed to be responsible for SGBS, Mateos et al. recently reported that GPC3 exon 2–4 duplication can cause SGBS [5]. This appears to be a second case of SGBS associated with GPC3 duplication.

Thus, postmortem MRI, autopsy, and molecular genetics represent complementary methods for the detailed evaluation of hereditary diseases.

Conflicts of interest

The authors have no conflicts of interest and received no financial support for this work.

References

[1] Chen CP. Prenatal findings and the genetic diagnosis of fetal overgrowth disorders: Simpson–Golabi–Behmel syndrome, Sotos syndrome, and Beckwith–Wiedemann syndrome. Taiwan J Obstet Gynecol 2012;51:186–91.
[2] Golabi M, Leung A, Lopez C, editors. Simpson–Golabi–Behmel Syndrome Type 1. GeneReviews™ [Internet]. Washington: University of Washington; 2006.
[3] Lequin MH, Huisman TA. Postmortem MR imaging in the fetal and neonatal period. Magn Reson Imaging Clin N Am 2012;20:129–43.
[4] Thayyil S, Sebire NJ, Chitty LS, et al. Post-mortem MRI versus conventional autopsy in fetuses and children: a prospective validation study. Lancet 2013;20:223–33.
[5] Mateos ME, Beyer K, López-Laso E, et al. Simpson–Golabi–Behmel syndrome type 1 and hepatoblastoma in a patient with a novel exon 2–4 duplication of the GPC3 gene. Am J Med Genet A 2013;161:1091–5.

Daigo Ochiai*
Department of Obstetrics & Gynecology, Saitama City Hospital, 2460 Mimuro, Midori-ku, Saitama-shi, Saitama 336-8522, Japan

Hirofumi Ohashi
Division of Medical Genetics, Saitama Children's Medical Center, 2100 Magome, Iwatsuki-ku, Saitamashi, Saitama 339-8551, Japan

Hiromi Hisazumi-Watanabe
Yoshiomi Sato
Department of Radiology, Saitama City Hospital, 2460 Mimuro, Midori-ku, Saitama-shi, Saitama 336-8522, Japan
Kazumi Yakubo
Tatsuro Fukuiya
Department of Obstetrics & Gynecology, Saitama City Hospital, 2460 Mimuro, Midori-ku, Saitama-shi, Saitama 336-8522, Japan

*Corresponding author. Tel.: +81 48 873 4111; fax: +81 48 873 5451
E-mail address: ochiaidaigo@gmail.com (D. Ochiai)

13 June 2013

http://dx.doi.org/10.1016/j.ejogrb.2013.09.044

ORIGINAL ARTICLE AJO-DO

Systemic and maxillofacial characteristics of patients with Beckwith-Wiedemann syndrome not treated with glossectomy

Akiko Kawafuji,[a] Naoto Suda,[b] Naoko Ichikawa,[c] Sumako Kakara,[d] Tsuyoshi Suzuki,[e] Yoshiyuki Baba,[f] Takuya Ogawa,[g] Michiko Tsuji,[h] and Keiji Moriyama[i]
Tokyo, Japan

Introduction: Beckwith-Wiedemann syndrome (BWS) is a genetic disorder characterized by exomphalos, macroglossia and gigantism. Previous studies reported a wide variation in the skeletal and occlusal characteristics in individuals affected by BWS. However, these studies were performed by analyzing both individuals who had and those had not received a glossectomy, which has a high impact on the jaw growth and occlusion. To highlight the intrinsic characteristics of BWS, 7 Japanese affected individuals without glossectomy were analyzed in this study. **Methods:** Seven individuals who had been diagnosed with BWS by medical specialists and had not undergone glossectomy were analyzed. Cephalograms and dental casts were taken and systemic complications were recorded at the first visit. **Results:** Individuals uniformly showed a higher birth height and weight, macroglossia, large anterior cranial base, and mandibular body. They exhibited a wide dental arch and an anterior open bite due to the undererupted and proclined anterior teeth. A wide variation was seen in the gonial angle, but the facial height was large overall. **Conclusions:** As intrinsic characteristics of BWS, individuals exhibited macroglossia resulting in an anterior open bite and a wide dental arch. A long facial height and an enlarged anterior cranial base and mandibular body were also noted. (Am J Orthod Dentofacial Orthop 2011;139:517-25)

Beckwith-Wiedemann syndrome (BWS) (MIM 130650) was reported by Beckwith and Wiedemann.[1,2] Beckwith reported 3 unrelated children with exomphalos (an umbilical hernia at birth in which some abdominal organs push into the umbilical cord), macroglossia, hyperplasia of kidneys and pancreas, hypoglycemia, and adenocortical cytomegaly.[1] Wiedemann independently reported siblings with exomphalos and macroglossia.[2] BWS is a congenital disease classified as one of the overgrowth syndromes and its occurrence is known to be 1/13,700.[3] Genes, such as *IGF2, H19, p57KIP2,* and *LIT1,* in an imprinted genomic domain of 11p15 are associated with this disease.[4] *IGF2* and *H19* are associated with cancer risk, and malignant tumors such as nephroblastoma, adrenal cortical carcinoma and hepatocellular carcinoma are frequently seen with this disease.[5]

Macroglossia is a predominant oral characteristic and is suggested to have a close relation to the oral function and maxillofacial morphology.[6-8] In many affected individuals, glossectomy is recommended to correct a swallowing and speech problem, chronic obstruction of the upper airway, and occlusion.[9,10]

Studies report a high prevalence of open bite in individuals affected by BWS, but inconsistencies are also reported in the maxillofacial morphology.[11-14] For instance, Masubuchi et al reported that an enlarged gonial angle and mandibular plane angle were uniformly seen in affected individuals.[12] In contrast, another study reported that the large gonial angle or steep mandibular plane angle was not seen.[14] Glossectomy is known to cause the reduction of mandibular length and width in animal

From Maxillofacial Orthognathics, Department of Maxillofacial Reconstruction and Function, Division of Maxillofacial/Neck Reconstruction, Graduate School of Medical and Dental Sciences, Tokyo Medical and Dental University, Tokyo, Japan.
[a]Resident.
[b]Lecturer.
[c]Resident.
[d]Resident.
[e]Resident.
[f]Assistant professor.
[g]Assistant professor.
[h]Assistant professor.
[i]Professor.
The authors report no commercial, proprietary, or financial interest in the products or companies described in this article.
Reprint requests to: Naoto Suda, Maxillofacial Orthognathics, Department of Maxillofacial Reconstruction and Function, Division of Maxillofacial/Neck Reconstruction, Graduate School, Tokyo Medical and Dental University, 1-5-45 Yushima, Bunkyo-ku, Tokyo, 113-8510, Japan; e-mail, n-suda.mort@tmd.ac.jp.
Submitted, February 2009; revised and accepted, July 2009.
0889-5406/$36.00

doi:10.1016/j.ajodo.2009.07.021

Table I. Systemic condition and complications in 7 Japanese individuals affected by Beckwith-Wiedemann syndrome

	Case 1	*Case 2*	*Case 3*	*Case 4*	*Case 5*	*Case 6*	*Case 7*
Sex	M	M	F	F	F	F	F
Fetal age at birth (week)	40	41	35	34	39	39	38
Birth height (cm)	52.3 (1.50)	55.0 (2.26)	46.8 (1.02)	48 (1.81)	Unknown	53 (2.59)	Unknown
Birth weight (g)	4,155 (3.13)	4,080 (2.26)	2,740 (1.65)	2,735 (3.09)	4,400 (3.85)	3,612 (1.92)	4,080 (3.87)
Present age (years)	4.8 years	8.6 years	6.3 years	6.8 years	7.5 years	8.5 years	9.2 years
Present height (cm)	105.1 (−1.18)	Unknown	115.3 (−0.08)	125.5 (2.01)	Unknown	122 (−0.98)	Unknown
Present weight (kg)	17.0 (−0.77)	Unknown	23.2 (0.63)	31.0 (2.93)	Unknown	23.8 (0.05)	Unknown
Present head circumference (cm)	50.0 (−0.50)	52.5 (0.42)	51.0 (0.39)	51.0 (0.39)	54.2 (2.62)	Unknown	Unknown
Macroglossia	1	1	1	1	1	1	1
Exomphalos	–	1	1	1	–	1	–
Tumor	–	–	–	–	1	–	1
Earlobe anomaly	–	1	–	1	–	Unknown	–
Hemihypertrophy	1	–	1	–	–	1	–

Each parenthesis in birth height/weight, present height/weight and head circumference denotes z score [(measurement − Japanese norm)/SD]. Each z score was evaluated by the sex- and age- (week) matched Japanese norms.[23-25]

studies.[8,15,16] Thus, although there is variability in this disease, we speculated that the analyses including both individuals who had and those who had not undergone glossectomy might be one of the reason for inconsistencies among these studies. The aim of this study is to highlight the intrinsic characteristics and to discuss the complications of a series of 7 cases affected by BWS.

MATERIAL AND METHODS

Seven Japanese individuals affected by BWS (2 male and 5 female) in our dental hospital were evaluated in this study. All 7 cases were diagnosed as BWS by medical specialists in multiple medical hospitals based on comprehensive and precise examination. Differential diagnosis was performed by the precise consideration on each case. Their ages at the first visit to our dental hospital ranged from 4 years 8 months to 9 years 2 months. Records on systemic conditions and complications—including birth height and weight, gestational week at birth, macroglossia, glossectomy, exomphalos, tumor, earlobe anomaly, and hemihypertrophy—were obtained by an inspection and an interview of patients and their parents. The present height, weigh,t and head circumference were measured at the first visit.

Cephalograms were obtained for all patients at the first visit, and the skeletal and dental characteristics were evaluated. Traditional cephalometric landmarks[17-20] were used in this study. Each overbite was measured from cephalograms. Every measurement of cephalograms was performed by 1 experienced orthodontist (A.K.). To minimize error, each measurement was repeated at least twice. Every error in measurement was within 6 0.5° degree or 0.5 mm.

Cast models were also taken in all patients at the first visit, and dental arch width and length were measured by caliper (type N•N-W, Mitutoyo, Tokyo, Japan), which had 6 0.05-mm error. The dental arch width, the distance between the tips of buccal cusps of the right and left teeth (deciduous canine and first and second molars, were measured in both arches.[21] The dental arch length, the distance from the contact point of deciduous central incisors to the line connecting the distal surfaces of the right and left deciduous second molars, were measured in both arches.[21] Every measurement of cast models was performed by 1 experienced orthodontist (T.S.). To minimize error, each measurement was repeated at least twice. Every error in measurements was within 6 0.5 mm.

The following norms were used in this study. Since individuals affected by BWS tend to be born prematurely,[22] the birth height and weight of the study individuals were evaluated by the norm at the corresponding gestational week of Japanese infants who had normal or preterm birth, as reported by The Ministry of Health, Labor and Welfare.[23] Norms of the height and weight of Japanese students were reported by The Ministry of Education, Culture, Sports, Science and Technology;[24] the norm of the Japanese head circumference by Ishikawa et al [25]; the Japanese norms of N-Me, N-ANS, ANS-Me, N-S, S-Ba, ANS-PNS, Ar-Go, and Go-Pog by Masaki[17]; the Japanese norms of SNA angle, U1 to FH, facial angle, SNB angle, mandibular plane angle, gonial angle, L1 to mandibular plane, and A-B plane angle by Iizuka[18]; the Japanese norms of ANS-Ar-U1 and Gn-Ar-L1 by Kamiyama[19], and the norm of N-S-Ar reported by Björk.[20] The norms of Japanese dental arch width and length were reported by Otsubo et al.[21]

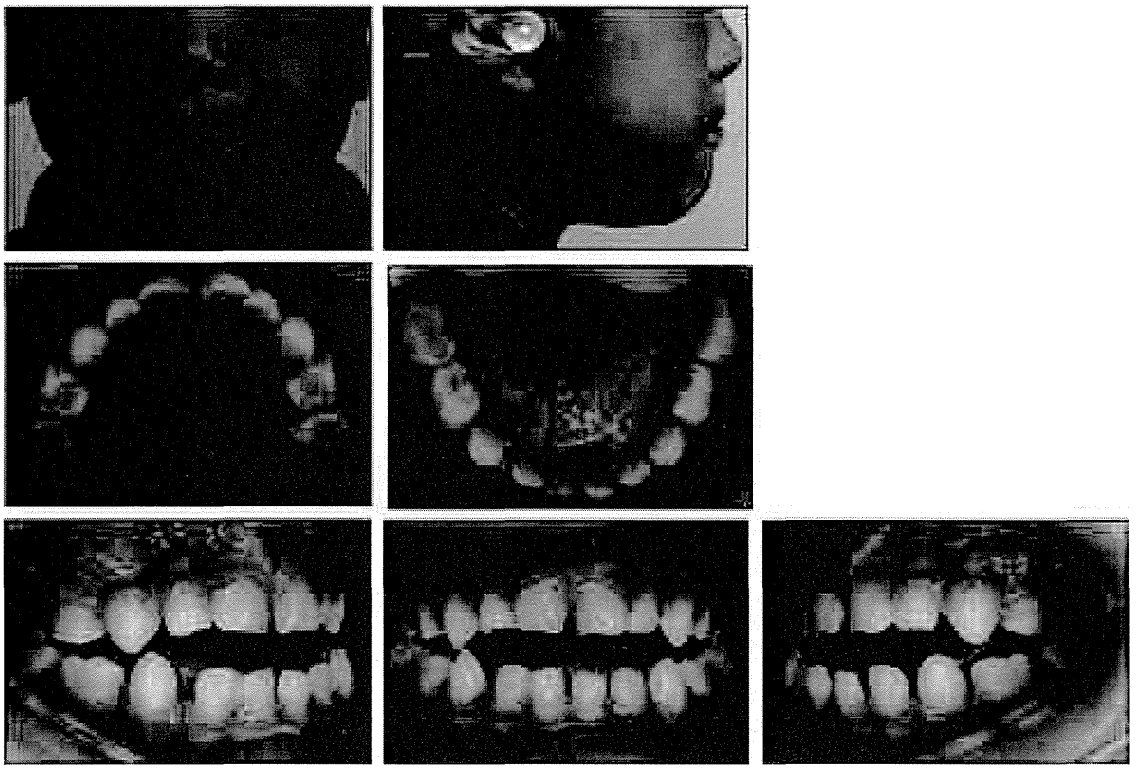

Fig 1. Facial and oral photographs of a typical individual affected by BWS (denoted as case 1 in Fig 2 and tables).

RESULTS

Systemic condition and complications in 7 individuals affected by BWS

The birth height was more than 1 SD higher than the Japanese week- and gestational week–matched norm in all 5 individuals who had that record (cases 1, 2, 3, 4, and 6) (Table I). Among them, 2 (cases 2 and 6) were more than 2 SD higher than the norm. The birth weight was more than 1 SD higher than the Japanese sex– and gestational week–norm in all 7 individuals. Among them, case 2 was more than 2 SD higher and cases 1, 4, 5, and 7 were more than 3 SD higher than the norm.

The present height and weight were more than 2 SD higher than the Japanese sex- and age-matched norm in 1 (case 4) of 4 individuals on record (Table I). The remaining 3 individuals were not higher than the norm. It was noted that most individuals who had high values in the birth height and weight became comparable to the Japanese norm; the exception was case 4.

The present head circumference was large in case 5 (*z* score, 2.62), but those of the remaining 4 individuals on record were comparable to the sex- and age-matched norm (Table I). Macroglossia was seen in all 7 cases. Exomphalos, tumor, earlobe abnormality, and hemihypertrophy were present in 4, 2, 2, and 3 cases, respectively. In 3 hemihypertrophy cases, tongues were not asymmetrical.

Skeletal characteristics of 7 affected individuals

Like case 1 (Fig 1), all 7 individuals showed an anterior open bite (Fig 2). The apparent mandibular prognathism was seen in cases 1, 4, 6, and 7 (Fig 2). Case 1 exhibited typical features of this disease, such as long face, macroglossia, open bite and spaced arch. Because of the macroglossia, the lingual cusps of the mandibular molars were hardly seen (Fig 1). The cephalometric measurements of the 7 individuals are summarized in Table II and Fig 3. The total (N-Me) and lower (ANS-Me) facial height was more than 1 SD higher in 4 of 6 patients who could be evaluated by the Japanese norm (Table II, Fig 3). However, N-ANS varied among cases. The anterior cranial base (N-S) was more than 2 SD higher in 6 individuals who could be evaluated (cases 2 to 7) (Table II, Figs 2 and 3).

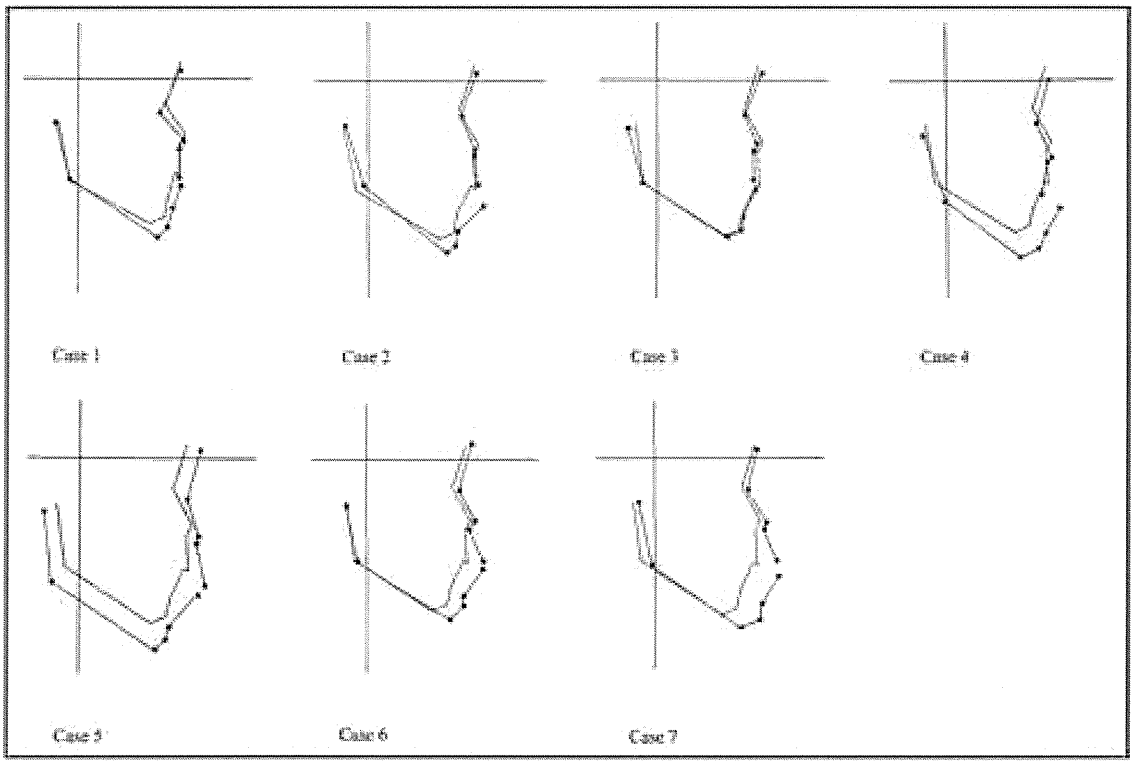

Fig 2. Profilograms[30] of 7 Japanese individuals affected by BWS. The Japanese age- and sex-matched norm is denoted by a solid line without a symbol in each profilogram.

Values of S-Ba and the saddle angle (N-S-Ar) varied among cases (Table II, Fig. 3).

For the maxilla, both ANS-PNS and SNA showed a variation, but the proclination of the maxillary incisors (U1 to FH plane) were uniformly seen (Table II, Fig 3). Undereruption (ANS-Ar-U1) of the maxillary incisors was clearly seen in cases 2 and 7.

For the mandible, although there was a variation in facial angle, SNB was more than 1 SD higher than the norm in 6 of 7 individuals, with the exception of case 5 (Table II, Fig 3). Go-Pog was more than 1 SD larger than the norm in 5 of 6 individuals who could be evaluated. The gonial angle showed a wide variation. Proclination (L1 to mandibular plane) and undereruption (Gn-Ar-L1) were uniformly seen in the mandibular incisors. Because of the variation in the SNA angle, there was a variation in the anterior-posterior relationship between maxilla and mandible (A-B plane) (Table II, Fig 3).

Dental arch of 7 affected individuals

The dental arch was measured in 7 individuals (Table III). Case 1 could not be evaluated because of the lack of the norm at 4 years of age. The distance between maxillary right and left deciduous canines in cases 3 and 6 was lower than the age-matched Japanese norm. However, measurable values of the dental arch width were higher overall than norms in cases 2 to 7.

The dental arch length was overall higher than the age-matched Japanese norm (Table III). *Z* scores of the mandible were higher than those of the maxilla in cases 2 to 7.

DISCUSSION

Three major conditions—exomphalos, macroglossia, and somatic gigantism—are frequently associated with BWS. In the present study, individuals showed increased birth weight compared with the Japanese norm (Table I). Among them, 4 of 7 individuals had more than 3-SD higher values. McManamny and Barnett reported only 9 of 30 individuals showed increased birth weight in Australian affected individuals.[9] The precise criteria of how they were defined as increased weight, or how many patients were born before 40 weeks of gestation is not known. In this study, since 5 individuals were born before 40 weeks of gestation, the birth weight

Table II. Cephalometric measures of 7 Japanese individuals affected with Beckwith-Weidemann syndrome

	Case 1	*Case 2*	*Case 3*	*Case 4*	*Case 5*	*Case 6*	*Case 7*
Facial height							
N-Me (mm)	105.9	113.1	105.3	114.4	121.1	113.8	114.1
	(ne)	(0.79)	(0.13)*	(2.40)*	(4.12)	(1.39)	(1.03)
N-ANS (mm)	45.3	47.5	44.2	50.1	49.6	50.1	46.7
	(ne)	(−0.69)	(−1.1)*	(1.46)*	(1.21)	(0.92)	(−1.79)
ANS-Me (mm)	63.3	66.9	62.1	67.3	75.0	65.7	69.6
	(ne)	(1.19)	(0.27)*	(1.59)*	(3.70)	(0.86)	(1.56)
Cranial base							
N-S (mm)	62.6	65.2	64.2	64.9	71.6	67.2	65.3
	(ne)	(2.61)	(3.36)*	(3.87)*	(8.08)	(3.68)	(2.11)
S-Ba (mm)	41.4	45.5	41.9	51.5	50.0	44.6	47.5
	(ne)	(−1.47)	(−2.68)*	(2.89)*	(2.11)	(−1.13)	(−1.05)
N-S-Ar (°)	124	125	127	113	129	121	114
	(0.2)	(0.4)	(0.8)	(−2.0)	(1.2)	(−0.4)	(−1.8)
Maxilla							
ANS-PNS (mm)	47.3	44.4	46	46.5	51.7	46.8	48.5
	(ne)	(−1.89)	(−0.83)*	(−0.55)*	(2.32)	(−1.03)	(−0.38)
SNA (°)	84	85	80.9	88.5	84	79.3	90.4
	(1.14)	(1.33)	(−0.16)	(2.17)	(0.80)	(−0.63)	(3.09)
U-1 to FH (°)	105.5	117.4	nm	nm	116.5	128.3	126.4
	(1.37)	(1.44)			(1.26)	(2.60)	(3.16)
ANS-A r -U1 (°)	16.5	14.2	nm	nm	16.3	16.0	14.02
	(−0.41)	(−1.80)			(−0.54)	(−0.72)	(−1.88)
Mandible							
Ar-Go (mm)	38.7	37.5	37.8	44.5	43.4	37.1	39.7
	(ne)	(−0.90)	(0.96)*	(2.36)*	(1.91)	(−1.36)	(−0.56)
Go-Pog (mm)	65.7	67.4	66.3	66.2	75.3	74.0	77.3
	(ne)	(0.61)	(1.41)*	(1.37)*	(4.8)	(4.06)	(4.30)
Facial angle (°)	85.4	83.2	83	86	80.1	86.9	90.9
	(0.28)	(0.02)	(0.03)	(0.68)	(−1.09)	(0.95)	(3.08)
SNB (°)	81.7	79.5	78.8	88.5	76.7	79.3	87.1
	(1.63)	(1.18)	(1.16)	(4.25)	(0.17)	(1.07)	(3.86)
Mandibular plane angle (°)	32.4	38.2	31.6	36.4	32.8	29.9	33.3
	(0.85)	(2.59)	(0.09)	(0.97)	(0.26)	(−0.31)	(0.55)
Gonial angle (°)	134.8	143.3	135.4	142	129	128.8	132.3
	(0.92)	(3.03)	(1.14)	(9.41)	(−0.90)	(−1.06)	(0.67)
L-1 to mandibular plane (°)	90.6	102.4	93.2	94.5	104.6	104.6	98.9
	(1.19)	(1.45)	(1.42)	(0.77)	(2.32)	(2.32)	(0.86)
Gn-Ar-L1 (°)	20.42	20.71	19.42	19.98)	20.36	20.99	19.46
	(−1.15)	(−1.00)	(−1.70)	(−1.39)	(−1.18)	(−0.83)	(−1.68)
Maxilla-Mandible							
ANB (°)	2.3	5.5	2.1	0.0	7.3	0.0	3.3
	(ne)	(ne)	(ne)	(ne)	(ne)	(ne)	(ne)
A-B plane (°)	−1.6	−5.7	−2.6	2.04	−7.3	−1.6	−2.8
	(1.70)	(0.56)	(1.92)	(3.60)	(−0.24)	(2.11)	(1.84)

N, nasion; *Me*, menton; *ANS*, anterior nasal spine; *S*, sella turcica; *Ba*, basion; *Ar*, articulare; *PNS*, posterior nasal spine; *A*, point A; *U-1*, long axis of maxillary central incisor; *U1*, tip of maxillary central incisal crown; *Go*, gonion; *Pog*, pogonion; *B*, point B; *L-1*, long axis of mandibular central incisor; *L1*, tip of mandibular central incisal crown; *Gn*, gnathion; *N-Me*, distance between N and Me; *N-ANS*, distance between N and ANS; *ANS-Me*, distance between and ANS and Me; *N-S*, distance between N and S; *S-Ba*, distance between S and Ba; *N-S-Ar*, angle between N-S and Ar; *ANS-PNS*, distance between ANS and PNS; *SNA*, angle between SN plane and N-A; *U-1 to FH*, angle between U-1 and FH plane; *ANS-Ar-U1*, angle between ANS, Ar, and U1; *Ar-Go*, distance between Ar and Go; *Go-Pog*, distance between Go and Pog; *Facial angle*, angle between FH plane and N-Pog; *SNB*, angle between SN plane and N-B; *Mandibular plane angle*, angle between mandibular plane and FH plane; *Gonial angle*, angle between mandibular plane and gonial plane; *L-1* to mandibular plane, angle between L-1 and mandibular plane; *Gn-Ar-L1*, angle between Gn, Ar, and L1; *ANB*; *SNA-SNB*, A-B plane, angle between N-Pog and A-B. Each number in parenthesis represents z score [(measurement − norm)/SD]. Each z score was evaluated by the sex- and age-matched norms, except N-S-Ar, ANS-Ar-U1 and Gn-Ar-L1, each of which has only 1 norm. The norms were those reported by Masaki[17] (N-Me, N-ANS, ANS-Me, N-S, S-Ba, ANS-PNS, Ar-Go, and Go-Pog), by Björk[20] (N-S-Ar), by Iizuka[18] (SNA, U1 to FH, facial angle, SNB, Mandibular plane angle, Gonial angle, L1 to Mandibular plane, A-B plane angle), and by Kamiyama[19] (ANS-Ar-U1 and Gn-Ar-L1). Z scores denoted by * were evaluated by the Japanese norm at 7 years because of the lack of norms at 6 years. nm, not measured because of the severe resorption of the deciduous upper incisal root; ne, not evaluated because of the lack of the Japanese sex- and age-matched norms.

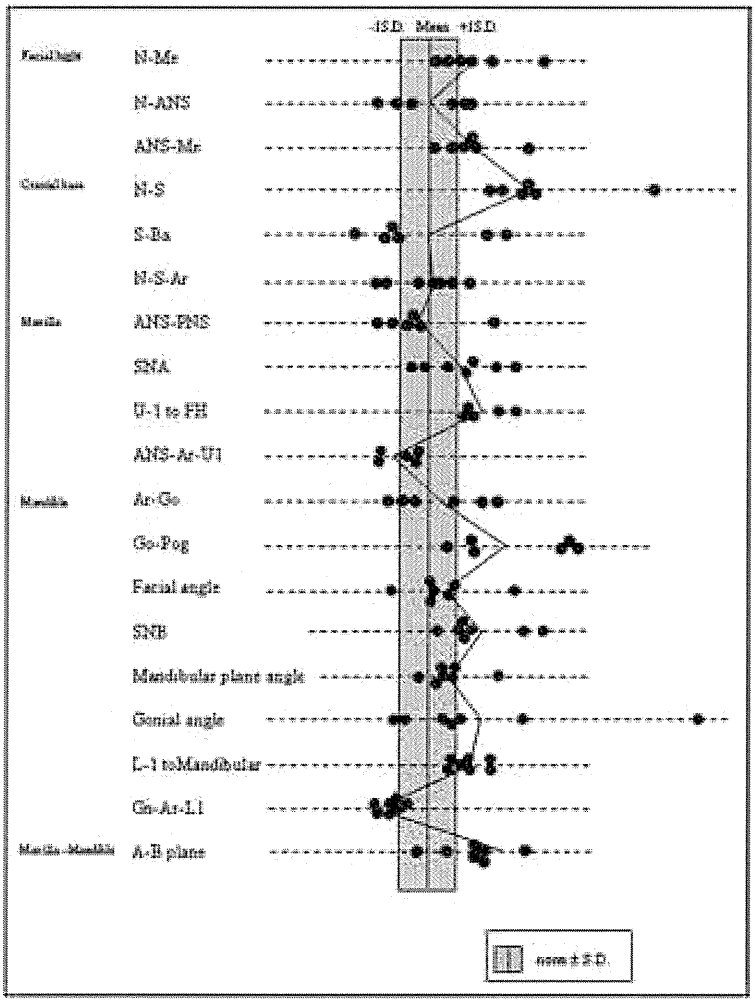

Fig 3. Skeletal characteristics of 7 Japanese individuals affected by BWS. *N,* nasion; *Me,* menton; *ANS*, anterior nasal spine; *S*, sella turcica; *Ba*, basion; *Ar*, articulare; *PNS*, posterior nasal spine; *A*, point A; *U-1*, long axis of maxillary central incisor; *U1*, tip of maxillary central incisal crown; *Go*, gonion; *Pog*, pogonion; *B*, point B; *L-1*, long axis of mandibular central incisor; *L1*, tip of mandibular central incisal crown; *Gn*, gnathion; *N-Me*, distance between N and Me; *N-ANS*, distance between N and ANS; *ANS-Me*, distance between ANS and Me N-, distance between N and S; *S-Ba*, distance between S and Ba; *N-S-Ar*, angle between N-S and Ar; *ANS-PNS*, distance between ANS and PNS; *SNA*, angle between SN plane and N-A; *U-1 to FH*, angle between U-1 and FH plane; *ANS-Ar-U1*, angle between ANS, Ar and U1; *Ar-Go*, distance between Ar and Go' Go-Pog, distance between Go and Pog; *Facial angle*, angle between FH plane and N-Pog; *SNB*, angle between SN plane and N-B; *Mandibular plane angle*, angle between mandibular plane and FH plane; *Gonial angle*, angle between mandibular plane and gonial plane; *L-1 to mandibular plane*, angle between L-1 and mandibular plane; *Gn-Ar-L1*, angle between Gn, Ar, and L1; *A-B plane*, angle between N-Pog and A-B. Each number in parenthesis represents *z* score [(measurement – norm)/SD]. Each *z* score was evaluated by the sex- and age-matched norms, except N-S-Ar, ANS-Ar-U1, and Gn-Ar-L1, each of which has only 1 norm. The norms were those reported by Masaki[17](N-Me, N-ANS, ANS, Me, N-S, S-Ba, ANS-PNS, Ar-Go, and Go-Pog), by Björk[20] (N-S-Ar), by Iizuka[18](SNA, U1 to FH, facial angle, SNB, Mandibular plane angle, Gonial angle, L1 to Mandibular plane, A-B plane angle), and by Kamiyama[19] (ANS-Ar-U1 and Gn-Ar-L1). Cases 3

Table III. Dental arch width and length of 7 Japanese individuals affected with Beckwith-Weidemann syndrome

	Case 1	*Case 2*	*Case 3*	*Case 4*	*Case 5*	*Case 6*	*Case 7*
Dental arch width							
Maxilla							
C-C (mm)	28.8	34.6	29.0	33.8	36.7	32.8	36.5
	ne	(1.28)	(−3.67)	(3.49)	(7.80)	(−0.52)	(4.45)
D-D (mm)	28.4	nm	31.7	32.2	38.1	33.8	nm
	ne		(0.34)	(1.02)	(8.47)	(0.67)	
E-E (mm)	33.0	40.6	38.7	39.3	41.9	38.6	39.7
	ne	(5.23)	(2.71)	(3.37)	(6.72)	(1.95)	(2.39)
Mandible							
C-C (mm)	30.2	30.6	27.2	29.1	28.9	nm	nm
	ne	(7.40)	(4.62)	(7.68)	(5.02)		
D-D (mm)	29.5	32.0	30.9	32.7	33.3	30.4	31.7
	ne	(5.47)	(6.42)	(9.38)	(7.69)	(2.71)	(3.84)
E-E (mm)	33.1	34.6	33.9	35.8	37.9	33.1	35.4
	ne	(2.92)	(3.96)	(6.53)	(8.52)	(1.28)	(2.78)
Dental arch length							
Maxilla	29.0	27.5	26.0	26.0	32.0	30.5	30.0
	ne	(−0.35)	(0.77)	(0.77)	(11.19)	(6.17)	(3.39)
Manible	30.0	32.0	26.0	28.0	28.5	29.0	27.0
	ne	(19.97)	(3.89)	(6.18)	(11.63)	(12.28)	(6.11)

Dental arch width was measured between the tips of both sides of the decidous canines *(C)* and between the mesial lingual cusps of both sides of the decidous first *(D)* and second *(E)* molars. Each number in parenthesis represents the z score [(measurement − norm)/SD]. Each z score was evaluated by the age-matched norm reported by Otsubo.[21] *nm*, not measured because of the shedding; *ne*, not evaluated because of the lack of the age-matched norm.

was evaluated by the sex- and gestational week–matched Japanese norm.[23] This would likely be the reason why the number of heavy patients was larger in this study than in the study of McManamny and Barnett.[9] All 7 individuals showed macroglossia in the present study (Table I). This is consistent with the high prevalence previously reported by McManamny and Barnett (100%)[9] and Engström et al (82.0%).[10] The higher birth height and weight were normalized with age (Table I). This is frequently seen in this anomaly.[10,22]

The prevalence of exomphalos (4 in 7 individuals) and earlobe anomalies (2 in 6 individuals) did not differ much from the previous studies reporting each condition as 72.0% and 38.0%, respectively.[10,22] Exomphalos is one of 3 major complications of this disease, but 28% of cases lack this symptom. Tumor (2 in 7 individuals) and hemihypertrophy (3 in 7 individuals) were reported as 7.5% and 12.6%, respectively.[10,26]

The present head circumference was long in only 1 individual (case 5) (Table I), but a long anterior cranial base (N-S) was noted in 6 individuals in whom this parameter could be evaluated (Table II, Fig 2). The embryonic cranial base is fully cartilaginous and formed by the fusion of the parachordal plates around the notochord.[27] During the postnatal period, endochondral ossification of the synchondrosis contributes largely to the expansion of the ossification centers and growth of the cranial base. It is proposed that the pathogenesis of BWS is mainly explained by the following 3 mechanisms:[4]

- Loss of imprinting of *IGF2* encoding insulin-like growth factor II, resulting in the activation of the normally silent maternally inherited allele of this gene
- Abnormal methylation of the normally unmethylated maternal allele of a differentially methylated region (DMR) upstream of the *H19* gene
- The paternal uniparental disomy of chromosome 11p15, in which the maternal copy is replaced with a duplicated paternal copy

All these result in the activation of *IGF2* expression, which promotes cartilage growth during the fetal and early postnatal period[28] and would account for the long cranial base in the present BWS patients.

and 4 were evaluated by the Japanese norm at 7 years because of the lack of that norm at 6 years. The linear measurements (N-Me, N-ANS, ANS, Me, N-S, S-Ba, ANS-PNS, Ar-Go, and Go-Pog) of case 1 were not included because of the lack of sex- and age-matched Japanese norms. The values of U-1 to FH and ANS-Ar-U1 in 2 cases (cases 3 and 4) were not included because of the severe root resorption of the deciduous upper incisors.

It was noted that the mandibular body length (Go-Pog) was quite large, but the maxillary length (ANS-PNS) was not (Table II, Fig 3). The maxilla and mandible are both membrane bones, but the growth of the latter is assisted by condylar, coronoid, and symphyseal cartilages.[29] The enlarged mandibular body might be due to the mandibular cartilaginous growth activated by *IGF2* expression. Another possible factor for enlargement of the mandibular body would be a mechanical effect of the tongue, which tends to bring the mandible to a forward and downward direction.

In the present study, overall large values were seen in the anterior cranial base (N-S), in the total (N-ANS) and lower (ANS-Me) facial height, and in the mandibular body (Go-Pog) (Table II, Figs 2 and 3). The proclination and undereruption of the anterior teeth, resulting in the anterior open bite, were commonly seen in all individuals. However, there was variation in the values of N-ANS, S-Ba, SNA angle, Ar-Go, gonial angle, and A-B plane angle. Among them, a considerable variation was seen in the gonial angle (Table II, Figs 2 and 3). In contrast to this finding, Masubuchi et al.reported that an enlarged gonial angle was uniformly seen in all 8 of that study's affected individuals, including 7 patients who had undergone glossectomy.[12] This discrepancy might be due to the difference in the skeletal pattern between affected individuals who had and those who had not undergone glossectomy. However, it is necessary to examine a larger number of affected individuals together with a precise record on the extent and size of the macroglossia and glossectomy. Moreover, it has to be noted that the tongue size is not the only factor that can affect the skeletal pattern. The tongue position and habit and the muscle activity could also worsen the skeletal pattern of BWS.

Some severely affected patients with extreme macroglossia would inevitably have glossectomies at a younger age. It has to be noted that the cases in this study would exclude these extremely severe cases.

CONCLUSIONS

Since macroglossia has a high impact on the jaw growth and occlusion, the intrinsic characteristics of BWS without glossectomy were examined in this study. The enlarged anterior cranial base and mandibular body were seen in all affected individuals. They exhibited a wide dental arch and an anterior open bite possibly due to the undererupted and proclined anterior teeth. A long facial height was also noted in this anomaly.

REFERENCES

1. Beckwith JB. Extreme cytomegaly of the adrenal fetal cortex, omphalocele, hyperplasia of the kidneys and pancreas, and Leydig cell hyperplasia — another syndrome? Presented at the annual meeting of the Western Society for Pediatric Research, Los Angeles, CA, 1963.
2. Wiedemann HR. Complex malformatif famililial avec hernie ompilicale et macroglossie. Un syndrome noveau? J Genet Hum 1964; 13:223-32.
3. Thorburn MJ, Wright ES, Miller CG, Smith-Read EHM. Exomphalos-macroglossia-gigantism symdrome in Jamaican infants. Am J Dis Child 1970;119:316-21.
4. Debaun MR, Feinberg AP. IGF2, H19, p57KIP2, and LIT1 and the Beckwith-Wiedemann syndrome. In: Epstein CL, Erickson RP, Wynshaw-Boris A, editors. Inborn errors of development. New York: Oxford University Press; 2004. p. 758-65.
5. Gorlin RJ, Cohen MM Jr, Hennnekam RCM. Overgrowth syndromes and postnatal onset obesity syndromes. In: Gorlin RJ, Cohen MM Jr., Hennnekam RCM, editors. Syndromes of the head and neck. 4th ed. New York: Oxford University Press; 2001. p. 399-427.
6. Giancotti A, Romanini G, Di Girolamo R, Arcuri C. A less-invasive approach with orthodontic treatment in Beckwith-Wiedemann patients. Orthod Craniofac Res 2002;5:59-63.
7. Friede H, Figueroa AA. The Beckwith-Wiedemann syndrome: a longitudinal study of the macroglossia and dentofacial complex. J Craniofac Genet Dev Biol 1985;1:179-87.
8. Liu ZJ, Shcherbatyy V, Gu G, Perkins JA. Effects of tongue volume reduction on craniofacial growth: a longitudinal study on orofacial skeletons and dental arches. Arch Oral Biol 2008;53:991-1001.
9. McManamny DS, Barnett JS. Macroglossia as a presentation of the Beckwith-Wiedemann syndrome. Plast Reconstr Surg 1985;75:170-6.
10. Engström W, Lindham S, Schofield P. Wiedemann-Beckwith syndrome. Eur J Pediatr 1988;147:450-7.
11. Rm, Delaire J, Schendel SA. Treatment of the craniofacial complications of Beckwith-Wiedemann syndrome. Plast Reconstr Surg 1995;96:27-33.
12. Masubuchi M, Sueishi K, Sakamoto T, Negishi F, Yamaguchi H. Orthodontic evaluation of eight cases in Beckwith-Wiedemann syndrome. Orthod Waves 2006;65:9-14.
13. Miyawaki S, Oya S, Noguchi H, Takano-Yamamoto T. Long-term changes in dentoskeletal pattern in a case with Beckwith-Wiedemann syndrome following tongue reduction and orthodontic treatment. Angle Orthod 2000;70:326-31.
14. Nakamura T, Kuroda T, Takagi Y. 4 cases of Beckwith-Wiedemann syndrome. J Jpn Orthod Soc 1986;45:286-94.
15. Schumwcher GH, Becker R, Hubner A, Pommerenke F. The tongue as a factor in craniofacial growth. 1. Modification of the linear dimensions of the lower jaw. Anat Anz 1988;166:1-5.
16. Becker R, Hubner A, Pommerenke F, Schumacher GH. The tongue as a factor in craniofacial growth. 2. The influence of the width dimension of the lower jaw. Anat Anz 1988;167:81-6.
17. Masaki F. [The longitudinal study of morphological differences in the cranial base and facial structure between Japanese and American whites.]. Nippon Kyosei Shika Gakkai Zasshi 1980;39:436-56.
18. Iizuka T. Roentgencephalometric analysis of craniofacial growth in Japanese children. J Stomatol Soc Jpn 1958;25:18-30.
19. Kamiyama T. Roentgenocephalometric analysis of open bite. J Jpn Orthod Soc 1958;17:31-40.
20. Björk A. The face in profile: an anthropological x-ray investigation on Swedish children and conscripts. Am J Orthod 1948;34:691-9.
21. Otsubo J, Ishikawa F, Kuwahara Y. A longitudinal study of dental development between 6 to 13 year of age. J Jpn Orthod Soc 1964; 23:182-90.

22. Elliott M, Maher ER. Beckwith-Wiedemann syndrome. J Med Genet 1994;31:560-4.
23. National growth survey of Japanese infants and children 2000. Ministry of Health, Labor and Welfare. Available at: http://www.mext.go.jp/b_menu/toukei/001/003/18/07031614/002.htm. Accessed October 24, 2001.
24. Physical development of students 2006. Ministry of Education, Culture, Sports, Science and Technology. Available at: http://www.mhlw.go.jp/houdou/0110/h1024-4.html. Accessed March, 2006.
25. Ishikawa T, Furukawa M, Ishikawa M, Ogawa J, Wada Y. Growth in head circumference from birth to fifteen years of age in Japan. Acta Pediatr Scand 1987;76:824-8.
26. Wiedemann HR. Tumours and hemiphypertrophy associated with Wiedemann Beckwith syndrome. Eur J Pediatr 1983;141:129.
27. Hoyte DA. The cranial base in normal and abnormal skull growth. Neurosurg Clin N Am 1991;2:515-37.
28. Canalis E. Effect of growth factors on bone cell replication and differentiation. Clin Orthop Relat Res 1985;193:246-63.
29. Nanci A. Embryology of the head, face, and oral cavity. In: Nanci A, editor. Ten Cate's Oral Histology-Development, Structure, and Function. 7th ed. St. Louis: Mosby; 2007. p. 32-56.
30. Sakamoto T. A study on the developmental changes of dentofacial complex of the Japanese with special reference to sella turcica. J Jpn Orthod Soc 1959;18:1-17.

Journal of Human Genetics (2011) 56, 91–93

www.nature.com/jhg

SHORT COMMUNICATION

Androgenetic/biparental mosaicism in a girl with Beckwith–Wiedemann syndrome-like and upd(14)pat-like phenotypes

Kazuki Yamazawa[1,5], Kazuhiko Nakabayashi[2], Kentaro Matsuoka[3], Keiko Masubara[1], Kenichiro Hata[2], Reiko Horikawa[4] and Tsutomu Ogata[1]

This report describes androgenetic/biparental mosaicism in a 4-year-old Japanese girl with Beckwith–Wiedemann syndrome (BWS)-like and paternal uniparental disomy 14 (upd(14)pat)-like phenotypes. We performed methylation analysis for 18 differentially methylated regions on various chromosomes, genome-wide microsatellite analysis for a total of 90 loci and expression analysis of *SNRPN* in leukocytes. Consequently, she was found to have an androgenetic 46,XX cell lineage and a normal 46,XX cell lineage, with the frequency of the androgenetic cells being roughly calculated as 91% in leukocytes, 70% in tongue tissues and 79% in tonsil tissues. It is likely that, after a normal fertilization between an ovum and a sperm, the paternally derived pronucleus alone, but not the maternally derived pronucleus, underwent a mitotic division, resulting both in the generation of the androgenetic cell lineage by endoreplication of one blastomere containing a paternally derived pronucleus and in the formation of the normal cell lineage by union of paternally and maternally derived pronuclei. It appears that the extent of overall (epi)genetic aberrations exceeded the threshold level for the development of BWS-like and upd(14)pat-like phenotypes, but not for the occurrence of other imprinting disorders or recessive Mendelian disorders.
Journal of Human Genetics (2011) **56,** 91–93; doi:10.1038/jhg.2010.142; published online 11 November 2010

Keywords: androgenesis; Beckwith–Wiedemann syndrome; mosaicism; upd(14)pat

INTRODUCTION

A pure androgenetic human with paternal uniparental disomy for all chromosomes is incompatible with life because of genomic imprinting.[1,2] However, a human with an androgenetic cell lineage could be viable in the presence of a normal cell lineage. Indeed, an androgenetic cell lineage has been identified in six liveborn individuals with variable phenotypes.[3–7] All the androgenetic cell lineages have a 46,XX karyotype, and this is consistent with the lethality of an androgenetic 46,YY cell lineage.

Here, we report on a girl with androgenetic/biparental mosaicism, and discuss the underlying factors for the phenotypic development.

CASE REPORT

This patient was conceived naturally to non-consanguineous and healthy parents. At 24 weeks gestation, the mother was referred to us because of threatened premature delivery. Ultrasound studies showed Beckwith–Wiedemann syndrome (BWS)-like features,[8] such as macroglossia, organomegaly and umbilical hernia, together with polyhydramnios and placentomegaly. The mother repeatedly received amnioreduction and tocolysis.

She was delivered by an emergency cesarean section because of preterm rupture of membranes at 34 weeks of gestation. Her birth weight was 3730 g (+4.8 s.d. for gestational age), and her length 45.6 cm (+0.7 s.d.). The placenta weighed 1040 g (+7.3 s.d.).[9] She was admitted to a neonatal intensive care unit due to asphyxia. Physical examination confirmed a BWS-like phenotype. Notably, chest roentgenograms delineated mild bell-shaped thorax characteristic of paternal uniparental disomy 14 (upd(14)pat),[10] although coat hanger appearance of the ribs indicative of upd(14)pat was absent (Supplementary Figure 1). She was placed on mechanical ventilation for 2 months, and received tracheostomy, glossectomy and tonsillectomy in her infancy, due to upper airway obstruction. She also had several clinical features occasionally reported in BWS[8] (Supplementary Table 1). Her karyotype was 46,XX in all the 50 lymphocytes analyzed. On the last examination at 4 years of age, she showed postnatal growth failure and severe developmental retardation.

[1]Department of Molecular Endocrinology, National Research Institute for Child Health and Development, Tokyo, Japan; [2]Department of Maternal-Fetal Biology, National Research Institute for Child Health and Development, Tokyo, Japan; [3]Division of Pathology, National Medical Center for Children and Mothers, Tokyo, Japan and [4]Division of Endocrinology and Metabolism, National Medical Center for Children and Mothers, Tokyo, Japan
[5]Current address: Department of Physiology, Development & Neuroscience, University of Cambridge, Cambridge, UK.
Correspondence: Dr T Ogata, Department of Molecular Endocrinology, National Research Institute for Child Health and Development, 2-10-1 Ohkura, Setagaya, Tokyo 157-8535, Japan.
E-mail: tomogata@nch.go.jp
Received 9 September 2010; revised 18 October 2010; accepted 22 October 2010; published online 11 November 2010

MOLECULAR STUDIES

This study was approved by the Institutional Review Board Committee at the National Center for Child health and Development, and performed after obtaining informed consent.

Methylation analysis

We first performed bisulfite sequencing for the *H19*-DMR (differentially methylated region) and KvDMR1 as a screening of BWS[11,12] and that for the IG-DMR and the *MEG3*-DMR as a screening of upd(14)pat,[10] using leukocyte genomic DNA. Paternally derived clones were predominantly identified for the four DMRs examined (Figure 1a). We next performed combined bisulfite restriction analysis for multiple DMRs, as reported previously.[13] All the autosomal DMRs exhibited markedly skewed methylation patterns consistent with predominance of paternally inherited clones, whereas the *XIST*-DMR on the X chromosome showed a normal methylation pattern (Figure 1a).

Genome-wide microsatellite analysis

Microsatellite analysis was performed for 90 loci with high heterozygosities in the Japanese population.[14] Major peaks consistent with paternal uniparental isodisomy and minor peaks of maternal origin were identified for at least one locus on each chromosome, with the minor peaks of maternal origin being more obvious in tongue and tonsil tissues than in leukocytes (Figure 1b and Supplementary Table 2). There were no loci with three or four peaks indicative of chimerism. The frequency of the androgenetic cells was calculated as 91% in leukocytes, 70% in tongue cells and 79% in tonsil cells, although the estimation apparently was a rough one (for details, see Supplementary Methods).

Expression analysis

We examined *SNRPN* expression, because *SNRPN* showed strong expression in leukocytes (for details, see Supplementary Data). *SNRPN* expression was almost doubled in the leukocytes of this patient (Figure 1c).

DISCUSSION

These results suggest that this patient had an androgenetic 46,XX cell lineage and a normal 46,XX cell lineage. In this regard, both the androgenetic and the biparental cell lineages appear to have derived from a single sperm and a single ovum, because a single haploid genome of paternal origin and that of maternal origin were identified in this patient by genome-wide microsatellite analysis. Thus, it is likely that after a normal fertilization between an ovum and a sperm, the paternally derived pronucleus alone, but not the maternally derived pronucleus, underwent a mitotic division, resulting both in the generation of the androgenetic cell lineage by endoreplication of

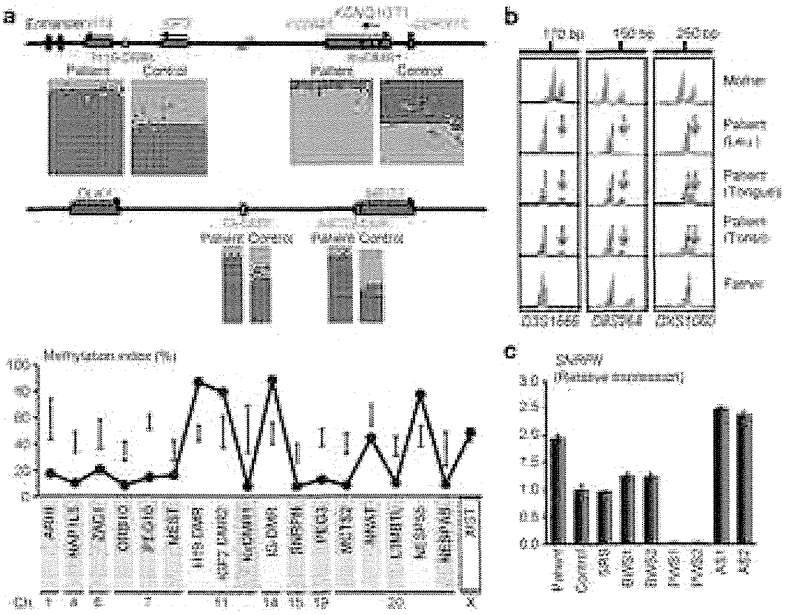

Figure 1 Representative molecular results. (**a**) Methylation analysis. Upper part: Bisulfite sequencing data for the *H19*-DMR and the KvDMR1 on 11p15.5, and those for the IG-DMR and the *MEG3*-DMR on 14q32.2. Each line indicates a single clone, and each circle denotes a CpG dinucleotide; filled and open circles represent methylated and unmethylated cytosines, respectively. Paternally expressed genes are shown in blue, maternally expressed gene in red, and the DMRs in green. The *H19*-DMR, the IG-DMR, and the *MEG3*-DMR are usually methylated after paternal transmission and unmethylated after maternal transmission, whereas the KvDMR1 is usually unmethylated after paternal transmission and methylated after maternal transmission.[10,11] Lower part: Methylation indices (the ratios of methylated clones) obtained from the COBRA analyses for the 18 DMRs. The DMRs highlighted in blue and pink are methylated after paternal and maternal transmissions, respectively. The black vertical bars indicate the reference data (maximum – minimum) in leukocyte genomic DNA of 20 normal control subjects (the *XIST*-DMR data are obtained from 16 control females). (**b**) Representative microsatellite analysis. Major peaks of paternal origin and minor peaks of maternal origin (red arrows) have been identified in this patient. The minor peaks of maternal origin are more obvious in tongue and tonsil tissues than in leukocytes (Leu.). (**c**) Relative expression level (mean ± s.d.) of *SNRPN*. The data are normalized against *TBP*. SRS: an SRS patient with an epimutation (hypomethylation) of the *H19*-DMR; BWS1: a BWS patient with an epimutation (hypermethylation) of the *H19*-DMR; BWS2: a BWS patient with upd(11)pat; PWS1: a Prader-Willi syndrome (PWS) patient with upd(15)mat; PWS2: a PWS patient with an epimutation (hypermethylation) of the *SNRPN*-DMR; AS1: an Angelman syndrome (AS) patient with upd(15)pat; and AS2: an AS patient with an epimutation (hypomethylation) of the *SNRPN*-DMR. The data were obtained using an ABI Prism 7000 Sequence Detection System (Applied Biosystems).

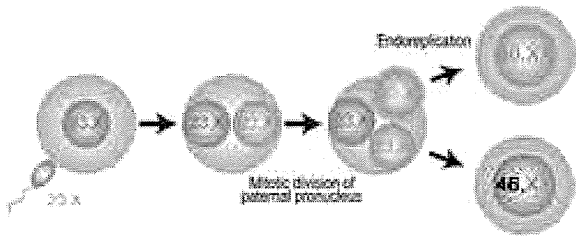

Figure 2 Schematic representation of the generation of the androgenetic/biparental mosaicism. Polar bodies are not shown.

one blastomere containing a paternally derived pronucleus and in the formation of the normal cell lineage by union of paternally and maternally derived pronuclei (Figure 2). This model has been proposed for androgenetic/biparental mosaicism generated after fertilization between a single ovum and a single sperm.[5,15,16] The normal methylation pattern of the *XIST*-DMR is explained by assuming that the two X chromosomes in the androgenetic cell lineage undergo random X-inactivation, as in the normal cell lineage. Furthermore, the results of microsatellite analysis imply that the androgenetic cells were more prevalent in leukocytes than in tongue and tonsil tissues.

A somatic androgenetic cell lineage has been identified in seven liveborn patients including this patient (Supplementary Table 1).[3–7] In this context, leukocytes are preferentially utilized for genetic analyses in human patients, and detailed examinations such as analyses of plural DMRs are necessary to detect an androgenetic cell lineage. Thus, the hitherto identified patients would be limited to those who had androgenetic cells as a predominant cell lineage in leukocytes probably because of a stochastic event and received detailed molecular studies. If so, an androgenetic cell lineage may not be so rare, and could be revealed by detailed analyses as well as examinations of additional tissues in patients with relatively complex phenotypes, as observed in the present patient.

Phenotypic features in androgenetic/biparental mosaicism would be determined by several factors. They include (1) the ratio of two cell lineages in various tissues/organs, (2) the number of imprinted domains relevant to specific features (for example, dysregulation of the imprinted domains on 11p15.5 and 14q32.2 is involved in placentomegaly[9,17]), (3) the degree of clinical effects of dysregulated imprinted domains (an (epi)dominant effect has been assumed for the 11p15.5 imprinted domains[18]), (4) expression levels of imprinted genes in androgenetic cells (although *SNRPN* expression of this patient was consistent with androgenetic cells being predominant in leukocytes, complicated expression patterns have been identified for several imprinted genes in both androgenetic and parthenogenetic fetal mice, probably because of perturbed *cis*- and *trans*-acting regulatory mechanisms[19]) and (5) unmasking of possible paternally inherited recessive mutation(s) in androgenetic cells. Thus, in this patient, it appears that the extent of overall (epi)genetic aberrations exceeded the threshold level for the development of BWS-like and upd(14)pat-like body and placental phenotypes, but remained below the threshold level for the occurrence of other imprinting disorders or recessive Mendelian disorders.

CONFLICT OF INTEREST

The authors declare no conflict of interest.

ACKNOWLEDGEMENTS

This work was supported by grants from the Ministry of Health, Labor, and Welfare, and the Ministry of Education, Science, Sports and Culture.

1 Surani, M. A., Barton, S. C. & Norris, M. L. Development of reconstituted mouse eggs suggests imprinting of the genome during gametogenesis. *Nature* **308,** 548–550 (1984).
2 McGrath, J. & Solter, D. Completion of mouse embryogenesis requires both the maternal and paternal genomes. *Cell* **37,** 179–183 (1984).
3 Hoban, P. R., Heighway, J., White, G. R., Baker, B., Gardner, J., Birch, J. M. *et al.* Genome-wide loss of maternal alleles in a nephrogenic rest and Wilms' tumour from a BWS patient. *Hum. Genet.* **95,** 651–656 (1995).
4 Bryke, C. R., Garber, A. T. & Israel, J. Evolution of a complex phenotype in a unique patient with a paternal uniparental disomy for every chromosome cell line and a normal biparental inheritance cell line. *Am. J. Hum. Genet.* **75**(Suppl), 831 (2004).
5 Giurgea, I., Sanlaville, D., Fournet, J. C., Sempoux, C., Bellanne-Chantelot, C. & Touati, G. Congenital hyperinsulinism and mosaic abnormalities of the ploidy. *J. Med. Genet.* **43,** 248–254 (2006).
6 Wilson, M., Peters, G., Bennetts, B., McGillivray, G., Wu, Z. H., Poon, C. *et al.* The clinical phenotype of mosaicism for genome-wide paternal uniparental disomy: two new reports. *Am. J. Med. Genet. Part A* **146A,** 137–148 (2008).
7 Reed, R. C., Beischel, L., Schoof, J., Johnson, J., Raff, M. L. & Kapur, R. P. Androgenetic/biparental mosaicism in an infant with hepatic mesenchymal hamartoma and placental mesenchymal dysplasia. *Pediatr. Dev. Pathol.* **11,** 377–383 (2008).
8 Jones, K. L. *Smith's Recognizable Patterns of Human Malformation* 6th edn. (Elsevier Saunders: Philadelphia, 2006).
9 Kagami, M., Yamazawa, K., Matsubara, K., Matsuo, N. & Ogata, T. Placentomegaly in paternal uniparental disomy for human chromosome 14. *Placenta* **29,** 760–761 (2008).
10 Kagami, M., Sekita, Y., Nishimura, G., Irie, M., Kato, F., Okada, M. *et al.* Deletions and epimutations affecting the human 14q32.2 imprinted region in individuals with paternal and maternal upd(14)-like phenotypes. *Nat. Genet.* **40,** 237–242 (2008).
11 Yamazawa, K., Kagami, M., Nagai, T., Kondoh, T., Onigata, K., Maeyama, K. *et al.* Molecular and clinical findings and their correlations in Silver-Russell syndrome: implications for a positive role of IGF2 in growth determination and differential imprinting regulation of the IGF2-H19 domain in bodies and placentas. *J. Mol. Med.* **86,** 1171–1181 (2008).
12 Weksberg, R., Shuman, C. & Beckwith, J. B. Beckwith-Wiedemann syndrome. *Eur. J. Hum. Genet.* **18,** 8–14 (2010).
13 Yamazawa, K., Nakabayashi, K., Kagami, M., Sato, T., Saitoh, S., Horikawa, R. *et al.* Parthenogenetic chimaerism/mosaicism with a Silver-Russell syndrome-like phenotype. *J. Med. Genet.* **47,** 782–785 (2010).
14 Ikari, K., Onda, H., Furushima, K., Maeda, S., Harata, S. & Takeda, J. Establishment of an optimized set of 406 microsatellite markers covering the whole genome for the Japanese population. *J. Hum. Genet.* **46,** 207–210 (2001).
15 Kaiser-Rogers, K. A., McFadden, D. E., Livasy, C. A., Dansereau, J., Jiang, R., Knops, J. F. *et al.* Androgenetic/biparental mosaicism causes placental mesenchymal dysplasia. *J. Med. Genet.* **43,** 187–192 (2006).
16 Kotzot, D. Complex and segmental uniparental disomy updated. *J. Med. Genet.* **45,** 545–556 (2008).
17 Monk, D., Arnaud, P., Apostolidou, S., Hills, F. A., Kelsey, G., Stanier, P. *et al.* Limited evolutionary conservation of imprinting in the human placenta. *Proc. Natl. Acad. Sci. USA.* **103,** 6623–6628 (2006).
18 Azzi, S., Rossignol, S., Steunou, V., Sas, T., Thibaud, N., Danton, F. *et al.* Multilocus methylation analysis in a large cohort of 11p15-related foetal growth disorders (Russell Silver and Beckwith Wiedemann syndromes) reveals simultaneous loss of methylation at paternal and maternal imprinted loci. *Hum. Mol. Genet.* **18,** 4724–4733 (2009).
19 Ogawa, H., Wu, Q., Komiyama, J., Obata, Y. & Kono, T. Disruption of parental-specific expression of imprinted genes in uniparental fetuses. *FEBS Lett.* **580,** 5377–5384 (2006).

Supplementary Information accompanies the paper on Journal of Human Genetics website (http://www.nature.com/jhg)